UNIVERSITY OF CALIFORNIA

Los Angeles

Closed-loop pulsed flash cooling for high heat flux electronics

A thesis submitted in partial satisfaction
of the requirements for the degree Master of Science
in Mechanical Engineering

by

Rishi Pugazhendhi

2023

ABSTRACT OF THE THESIS

Closed-loop pulsed flash cooling for thermal management of high heat flux electronics

by

Rishi Pugazhendhi
Master of Science in Mechanical Engineering
University of California, Los Angeles, 2023
Professor Timothy S. Fisher, Chair

As demand for high performance computing continues its rapid growth, the required digital processing capabilities necessitate more powerful integrated circuits. High power density chips produce a challenging thermal engineering problem by generating heat fluxes greater than 0.5 W/mm^2 while sometimes providing diminishing provisions for heat spreading. A pressure-driven boiling approach, termed flash cooling, is considered here as a solution for high heat flux thermal management. The thesis study aims to improve the Technology Readiness Level of flash cooling for high heat flux electronic cooling applications, especially targeted for wafer-scale systems. Furthermore, the objective is also extended to understand the physics involved in flash cooling and associated limitations. A closed-loop flash cooling system is developed with evaporator, accumulator, vacuum pump, condenser, and reservoir. Methanol is employed as an operating fluid. Experiments are conducted by varying the heat flux from 0.2 W/mm^2 to 1 W/mm^2 and the corresponding flow rate varies from 0.13 ml/s to 1 ml/s. The experiment is conducted for 1800 seconds to achieve steady periodic conditions. The results indicate that the steady periodic temperature of the evaporator was below 85 °C for heat fluxes up to 0.6 W/mm^2. The maximum oscillations in the evaporator temperature and pressure are determined to be ± 3.5 °C and 9 kPa,

respectively, for the heat flux corresponding to 1 W/mm^2. The crucial control parameter is determined to be pulse cycle time since the results suggest that a maximum feasible pulse cycle time exists for each heat flux above which conditions favoring stable vapor formation prevails. The maximum feasible pulse cycle time to avoid stable vapor formation is found to be 0.28 seconds for 1 W/mm^2. The correlations between control parameters are extrapolated and it can be utilized to ascertain the pulse cycle time and flow rate for a given heat flux to yield better cooling. The experiments not only prove the dynamic and transient cooling ability of pulsed flash cooling but also exhibit dry-out recovery characteristics under short pulse cycle times. Further research directions are also suggested to improve the flash cooling technology.

The thesis of Rishi Pugazhendhi is approved.

Subramanian S. Iyer

Vijay K Dhir

Timothy S. Fisher, Committee Chair

University of California, Los Angeles

2023

TABLE OF CONTENTS

LIST OF FIGURES

LIST OF TABLES

Acknowledgements

I extend my utmost respect and gratitude to my supervisor, Dr. Timothy S. Fisher, for his instrumental role in shaping me into a proficient researcher. His steadfast support and comprehensive guidance have been pivotal to my personal and academic development. I am sincerely thankful to my mentor, Dr. Subramanian S. Iyer, whose insightful perspectives, guidance, and thought-provoking discussions have significantly contributed to my growth. Once again, I express my heartfelt thanks to both of my advisors for granting me the privilege to delve into an inspiring research topic. I extend my gratitude to Dr. Vijay K Dhir for inspiring me with his teaching and guidance.

I wholeheartedly dedicate my thesis to Akshaya Suresh, my extraordinary other half, whose unwavering support has been the cornerstone of my journey through thick and thin. Her invaluable contributions have truly been the driving force behind my success.

I extend my sincere appreciation for the invaluable support, engaging discussions, and technical insights generously shared by Dr. Ujash Shah, Zachary Wong, Min Jong Kil, Haoxiang Ren and Naarendharan Meenakshi Sundaram. I heartfully thank the undergraduate students - Jesse Torres, Ben Yang, and Yini He - who contributed to my research. Furthermore, I express gratitude to UCLA for providing me with an enriching platform to apply and showcase my research skills. I extend my gratitude to Rajvikram Madurai Elavarasan for his sustained support and for introducing the enriching world of research into my life.

Finally, my heartfelt appreciation goes to my dearest parents, Pugazhendhi Ramasamy and Kalaivani Pugazhendhi, and my brother, Rajesh Pugazhendhi. Their unwavering trust and support have been the bedrock of my educational pursuits.

Chapter 1. Introduction

1.1. Motivation

Electronics cooling is developing into a field requiring state-of-the-art engineering capabilities to solve complex thermal management issues. Excessive temperature is the major reason for the failure of electronics [1]. Heat can reduce longevity, throttle performance, drain energy and cause customer discomfort. Thus, the thermal management of electronics is a critical aspect of the design and operation of semiconductor devices. Given the current trend of miniaturization and seamless integration, managing heat dissipation is increasingly challenging. Only upon solving the thermal challenges further miniaturization is possible on commercial grounds; thus, thermal management is a bottleneck issue for technological advancement. The problem becomes much more complicated when dealing with high-performance computing (HPC) devices requiring peak performance and heat dissipation. Moreover, total cooling system energy consumption accounts for about 30-40% of total electricity consumption in IT equipment and this number is projected to grow in upcoming years [2].

With the development in nanotechnology, high-density packaging of transistors is improving, and the trend is increasing following Moore's law which may be deviating in recent years. The development of chips with billions of transistors is simply a marvelous feat of engineering and the related thermal management technologies are also highly commendable. Fig 1 shows the increasing trend in power and heat flux dissipated by a chip [3]. In terms of heat flux, 2020 data corresponds to around 2 W/mm^2 of heat flux. On analyzing the commercial products, a recent high-performance computing NVIDIA H100 chip with a die size of 814 mm^2 has a maximum

thermal design power (TDP) of 700 W, yielding a peak heat flux of 0.86 W/mm^2 [4]. All these thermal challenges motivate to design required thermal solutions for future high heat flux products and their associated problems.

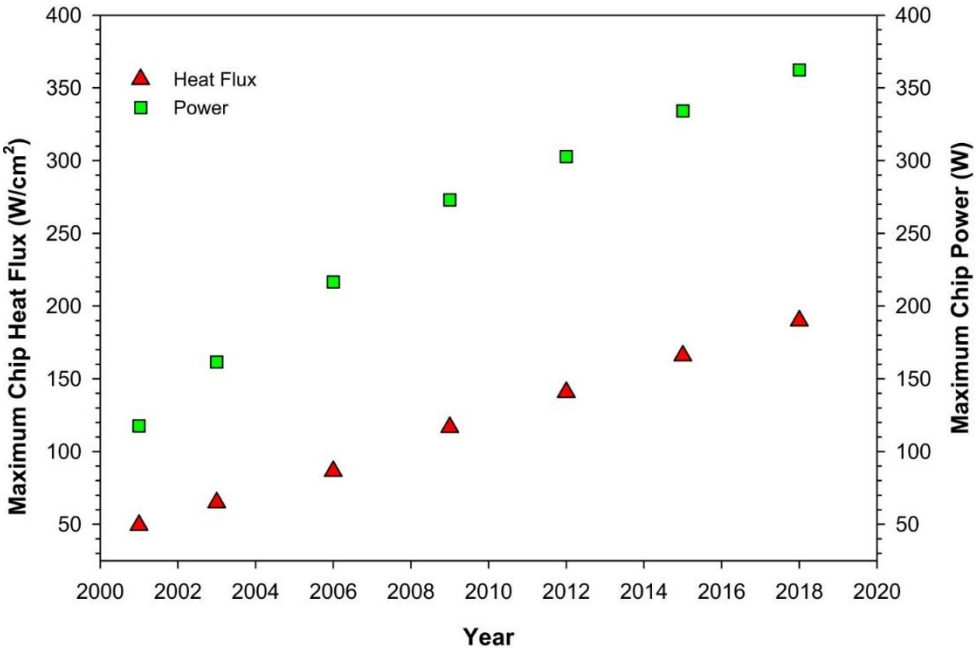

Fig. 1. Trends in maximum heat flux and power in chips up to 2020. Reproduced with permission from [3].

1.2. Thermal engineering challenges and objectives

High-performance computing devices find several applications ranging from data centers to supercomputers. The development of packaging techniques such as 2.5D, 3D and wafer-scale packaging techniques increases power density. From a thermal perspective, extracting the generated heat becomes difficult with limited heat spreading area for conventional thermal management solutions such as air cooling and direct liquid cooling. One such example is the Silicon Interconnect Fabric (Si-IF) developed by UCLA Chips Consortium. Si-IF is a large-scale

wafer system (300 mm wafer) built with fine-pitch die-to-wafer bonding [5,6] to achieve high computing power, large memory capacity and fast and efficient access to the memory. The design of the wafer-scale system is depicted in Fig 2. This large-scale wafer system can consume tremendous amounts of power, greater than 50 kW, while producing heat fluxes of 1 W/mm^2 or higher [7]. The active area can be as high as 60,000 mm^2 or more for a fully populated 300 mm wafer. The main challenge is not only intense heat generation but also little if any room for heat spreading area.

Heat spreading is critical to thermal management of electronics, the absence of which pushes the thermal engineering limits and requires alternative engineering approaches. From a thermal management perspective, the required heat transfer coefficient is about 17,000 W/(m^2 °C) (as shown in Eq. (1)) assuming that the allowable operating temperature of the chip is 85 °C and the ambient temperature is 25 °C.

$$h_{required} = \frac{q''}{T_s - T_\infty} = = 16.67 \text{ kW/(m}^2 \text{ °C)} \quad (1)$$

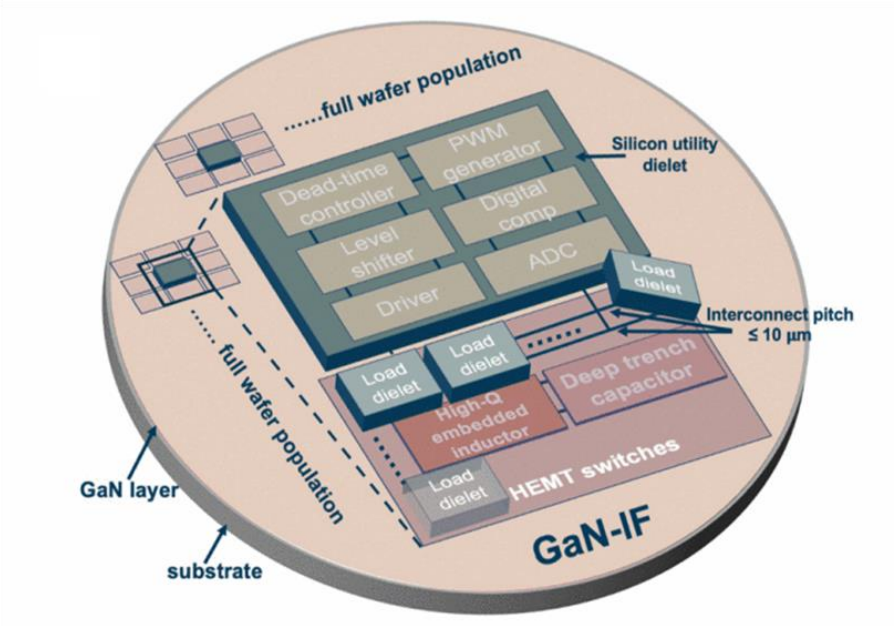

Fig. 2. Wafer-scale system designed by UCLA CHIPS consortium. Reproduced with permission from [7]

Even if there were provision for 2x heat spreading, the required heat transfer coefficient is in the range of 8500 W/(m^2 °C) and can be achieved by tuning the single-phase liquid cooling technique. Furthermore, with the advancement in packaging trends, it is possible to dissipate a peak heat flux of 3 W/mm^2. Air cooling is limited to a heat transfer coefficient 200 W/(m^2 °C) while the single-phase forced convective liquid cooling is limited to 7000 W/(m^2 °C) [8]. The only feasible thermal management solutions rely on two-phase liquid cooling technologies for which heat transfer coefficients can range from 3000 W/(m^2 °C) to 100,000 W/(m^2 °C) [8].

Wafer-scale systems induce the following unique problems in comparison to chip-scale solutions:

- ≥ 100X total heat removal (ranges in kW).
- Little if any heat spreading area.
- Traditional chip-scale solutions (e.g., microchannels) cooling are ineffective due to high-pressure drop, scalability, and cost.
- Requirement of segmented cooling and related packaging issues.
- Different chips in a wafer-scale system require various levels of transient response in a real-time operation.

Two-phase cooling technology is capable of handling such thermal management issues, but the conventional water flow boiling approach is not plausible because the saturation temperature of water at atmospheric pressure is greater than the required chip operating temperature (85 °C). Therefore, an alternative approach is required in two-phase technology. The thermodynamic properties, temperature and pressure of the liquid govern the boiling phenomenon. It is well known

that lowering pressure enables the boiling of liquids at lower temperatures. This will enhance the superheat, and effective two-phase cooling can be achieved. Depressurization-induced boiling forms the foundation for flash cooling where the liquid is boiled at a lower temperature.

This technology is relatively new to electronic cooling but its application can be extended to high heat flux and heat load data center cooling, thermal management in radar and battery systems, laser cooling, network switch, and single-use aerospace applications [9]. Apart from cooling applications, the flashing principle is also used for desalination [10]. When flash cooling is to be used for a high heat flux electronic cooling application, dynamic control and immediate transient response are required. Flash cooling technology is also applicable to areas where it does not require dynamic cooling. Flash cooling offers the flexibility to encounter transient heating, constant heat flux heating, and local hotspot cooling. The cooling configuration and dynamic control will be discussed in detail in upcoming chapters. To summarize, the objectives of the thesis work are as follows:

- To improve the Technology Readiness Level (TRL) for high heat flux electronic cooling applications.
- To engineer a closed-loop flash cooling system.
- To demonstrate cooling for a heat flux of ~1 W/mm^2 without heat spreading.
- To study and elucidate flash cooling behaviors as well as the physics involved.
- Identify the control parameters and assess their correlations with experimental data.

1.3. Literature review

A brief literature review has been performed to establish the research trends and physics involved in flash cooling. One study developed a vacuum spray flash cooling (VSFC) method for the

refrigeration application [11]. An experiment was performed for cooling a beverage, and it was found that VSFC cooled 6 times faster than a freezer. Another key finding suggests that flash cooling consists of two stages, where there is an initial enhancement providing a rapid cooling effect that is then followed by a gradual decline stage with a lower rate of cooling. Vacuum spray flash evaporation can remove heat effectively with a small flow rate. A study found that flash evaporation consumed about one-third of the flow rate used in the conventional spray cooling approach [12]. The experimental results also emphasize the influence of flow rates on heat removal. The heat transfer rate initially increases with the flow rate, and at an optimal flow rate the heat transfer is the highest followed by a decrease in heat transfer with a further increase in flow rate. Conversely, the heat transfer in the single-phase spray cooling always increases with the flow rate.

Peng and Cheng investigated the improvement in heat transfer with the use of Al_2O_3 nanoparticles in distilled water for vacuum spray flash evaporation cooling and reported that a uniform cooling profile is achieved [13]. To further enhance flash evaporation rates, surface modifications has been reported [14]. Kawano et al. performed numerical analysis on spray flash boiling on a multicomponent fuel system [15]. The authors showed numerically and experimentally that flash boiling enhances the atomization and vaporization of fuel droplets.

Vacuum flash evaporation from a spray cooling perspective can be categorized as film and droplet flash evaporation [16]. Film flash evaporation is the dominant mode of heat transfer where boiling occurs through heterogeneous nucleation by direct contact with the heated surface. On the other hand, droplet flash evaporation occurs before the liquid encounters the heated surface, possibly due to homogenous nucleation with sufficient superheat. The droplet evaporation reduces the temperature of the liquid before it reaches the heat source, thus increasing the cooling capacity.

However, a higher rate of droplet evaporation may result in dry-out conditions. Film flash evaporation is modeled based on film penetration theory while droplet flash evaporation is modelled based on diffusion-controlled evaporation model [17]. Guo and Zhu developed a modified lumped heat capacity model for predicting evaporating rates in droplet flashing [18]. The model aims to be as computationally simple as the Lumped Heat Capacity Model (LHCM) and as accurate as the Effective Heat Conduction Model (EHCM). The corrective factor is determined by assessing the evaporating rates of both EHCM and LHCM as a function of Fourier number.

Another study analyzed the effect of sudden depressurization on rapid evaporation of high-pressure R113 liquid [19]. The results show that bulk evaporation increases with an increase in pressure drop (depressurization). Similar to other studies focusing on evaporation by depressurization, two stages of decline in heat source temperature are observed – one being a rapid decline for an initial short duration and the other being a gradual decline for a longer duration. Aoki assessed the characteristics of flash evaporation of water at low-pressure conditions and obtained analytical expressions for maximum heat flux and heat transfer coefficient that was also validated with experiments [20].

Engerer et al. [21] reported that the flash boiling responds to depressurization within as little as 10 – 100 ms, and the experiments achieved a peak cooling of 30-50 W/cm^2 with temperature stability of ±5 °C up to an applied heat flux of 104 W/cm^2. Recently, flash boiling has been considered for transient thermal management of electronic devices involving power pulsations [22-24]. Shah et al. demonstrated a pulsed flash cooling approach for the thermal management of Si-IF as a solution for high-heat flux challenges with dynamic pulse control capabilities [25]. Frequent pulses exhibited lower temperatures and oscillations. A thesis by Ma determined that a minimum average superheat of around 5 °C is required for flash onset and found that pressure undershooting is crucial

in assessing local vaporization [26]. Shah et al. designed a convective evaporator chamber to facilitate rapid, transient flash cooling and utilized it for extracting heat from high-performance wafer-scale systems [27].

The literature review suggests that the flash boiling phenomenon has been studied most for spray cooling, and studies with pulsed flash approach do not exist according to the author's knowledge except from the same research group. An extensive study on flash boiling characteristics and control parameters exists as a knowledge gap for high heat flux conditions (> 0.5 W/mm^2). The proposed thesis aims to address the knowledge gap by elucidating the influence of control parameters on the pulsed flash boiling approach from both an engineering and physics perspectives.

The remainder of the study is structured as follows: Chapter 2 details the flash cooling experimental system covering its working principle, closed-loop experimental setup with component details, and design of experiments. Chapter 3 elaborates on the results achieved and the key findings. Chapter 4 summarizes the findings and concludes the study with future directions.

Chapter 2. Flash cooling experimental system

In this chapter, a detailed description of the flash cooling working principle and characteristics is covered. The chapter also elucidates the closed loop flash cooling architecture with an emphasis on individual components and data acquisition systems.

2.1. Flash cooling characteristics

The objective of the flash cooling system is to maximize heat transfer from the heat source to the operating fluid such that a minimum temperature is maintained at the heat source. This can be achieved with the utilization of the latent heat capacity of the operating liquid in addition to its sensible heat capacity. Any two-phase cooling approach can make use of the latent heat capacity of the coolant. However, the desired application of wafer-scale system introduces a constraint to maintain temperatures below 85 °C. The prime feature of flash cooling technology is that it enables the operating fluid to boil at a temperature lower than its boiling point at atmospheric pressure. This feature makes flash cooling more feasible for wafer-scale applications as well and it will enable higher quality by enriching wall superheat.

2.1.1. Working principle

Flash cooling adopts the principle of boiling driven by pressure control. Whenever a boiling phenomenon is concerned, two inter-related thermodynamic properties of the liquid define its feasibility and state of boiling: temperature and pressure. The principle used here is to reduce the pressure of the system (evaporator) such that the vapor pressure of the operating fluid is greater than the ambient pressure to facilitate boiling. This working principle is depicted in Fig 3. Flash cooling utilizes this phenomenon to boil the operating fluid by sudden depressurization.

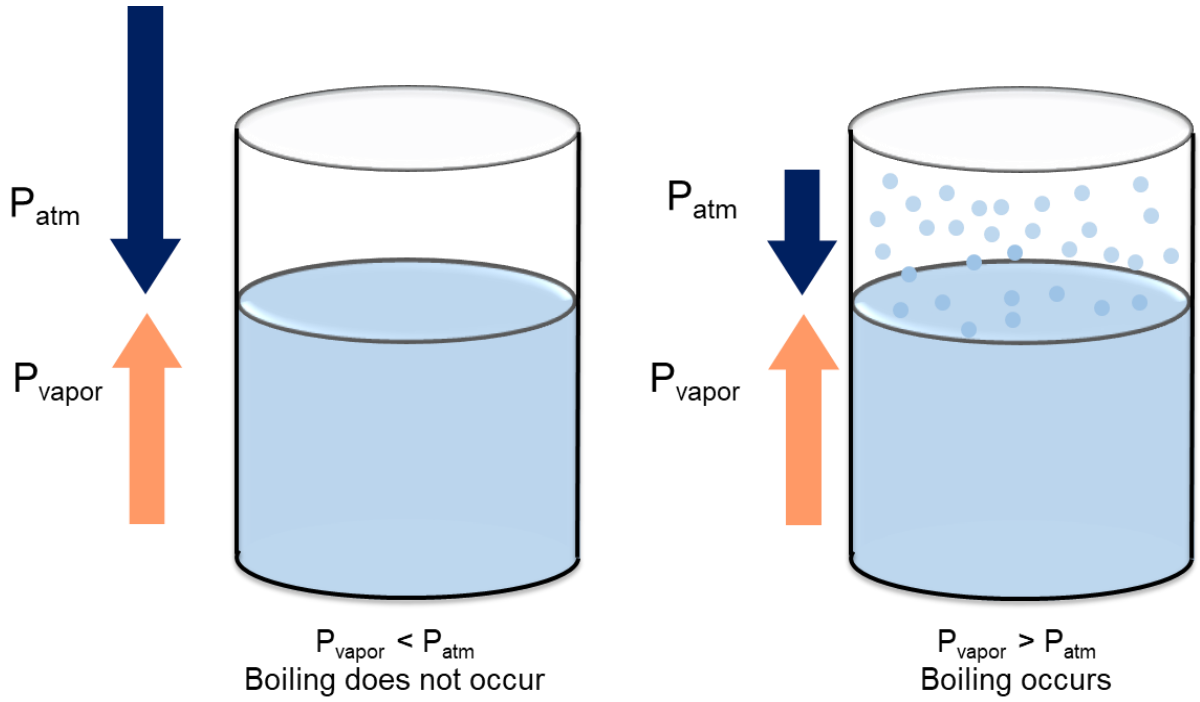

Fig. 3. Representation of flash boiling principle by depressurization of atmospheric pressure.

2.1.2. Pool flash boiling

Pool boiling is a boiling phenomenon that is accomplished by submerging a heated surface in a pool of liquid. Pool flash boiling essentially translates the same meaning, but the boiling is driven by depressurization such that the entire wall becomes a submerged heated surface. The proof of concept of the approach originated from research at Purdue University by Engerer and Fisher [28]. The experimental system consists of a transparent housing where a pool of methanol is stored. The heater is fixed below the porous graphitic foams which connect to the exit port. Upon depressurization, a sudden decrease in temperature occurs in the beginning, and the rate of cooling diminishes with time as shown in Fig 4. A significant feature of flash boiling is its high cooling rate during initial depressurization [29]. As the boiling continues, the vapor increases the overall

pressure in the chamber, and consequently, the rate of cooling decreases subsequently due to a decrease in the wall superheat. Pool flash boiling can also be utilized for desalination applications [30]. Further research has been carried out in pool flash boiling by Singh et al. who determined that increasing the initial temperature and pressure drop increases the cooling rate [31]. Both the temperature rise of the fluid and the large depressurization correspond to higher superheat availability.

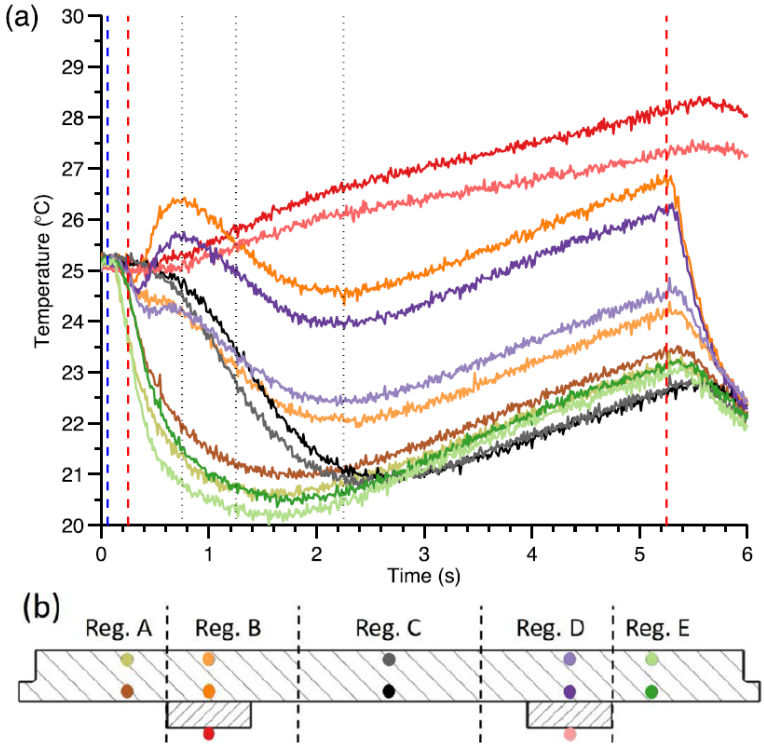

Fig. 4. Proof of concept for pool flash boiling (a) Temperature profile (b) Thermocouple location. Reprinted with permission from [28].

2.1.3. Flow flash boiling

Pool flash boiling cannot be effectively handled for cooling a wafer-scale system as the amount of cooling cannot be controlled accurately. Flow boiling induced by flashing would be an ideal solution for wafer-scale systems. The engineering hydraulic circuit for a flow flash boiling should be designed in a way that the fluid encounters sudden depressurization in the location where the heat is supplied. Consider a control volume where the liquid enters the control volume with a mass flow rate of $\dot{m}$ at P_L pressure and exits the control volume as a liquid vapor mixture at P_{LV} pressure. The heat flux, q'' is applied to the control volume as shown in Fig 5.

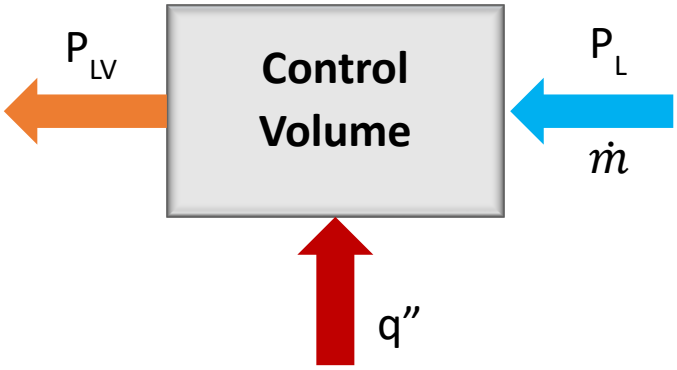

Fig. 5. Control Volume for Flow Flash Boiling.

Fig 5 suggests that a flow flash boiling can be accomplished by using two approaches. In the first approach, the liquid supplied to the control volume enters at high pressure and upon depressurization (free expansion), the induced pressure drop can cause flashing of liquid and the exit pressure of the liquid-vapor mixture can be near atmospheric pressure. Here the control volume exists at atmospheric conditions. Therefore, the condition for the first approach is $P_L >> P_{atm}$ and $P_{LV} \geq P_{atm}$. In the second approach, the control volume is maintained at a pressure below atmospheric pressure. The liquid supplied to the control volume enters at atmospheric pressure and

the exit pressure of the liquid-vapor mixture is lower than atmospheric pressure. Therefore, the condition for the second approach is $P_L = P_{atm}$ and $P_{LV} < P_{atm}$. The atmospheric pressure is the lowest in the first approach while it is the highest pressure in the second approach. A brief comparison between the two approaches is shown in Table 1.

Table 1. Comparison between the two approaches of flow flash boiling

Approach 1	**Approach 2**
Condition: $P_{LV} \geq P_{atm}$ & $P_L >> P_{atm}$	Condition: $P_{LV} < P_{atm}$ & $P_L = P_{atm}$
High-pressure liquid is depressurized to achieve flashing.	Liquid at atmospheric pressure is depressurized to achieve flash boiling
Control volume exists at atmospheric pressure	Control volume is maintained below atmospheric pressure
Compressor is required	Vacuum pump is required
Operating fluid should be a vapor at room temperature and pressure	Operating fluid should be a liquid at room temperature and pressure

The first approach is more similar to the vapor compression cycle with the only difference being that the throttling valve and evaporator are combined in a flow flash boiling cycle. Essentially, there would be only three thermodynamic states for a closed-loop flow flash boiling cycle in comparison to four thermodynamic states in a conventional vapor-compression refrigeration cycle.

Higher pressure requires less latent heat to accomplish the phase change from liquid to vapor. To extract more heat from the heat source through latent heat, a lower operating pressure is preferred. In other words, the control volume should be maintained at a lower pressure as possible. This makes the second approach better than the first approach in terms of enhancing flashing performance and higher cooling rates. Therefore, the proposed system will utilize a vacuum pump, condenser, reservoir and evaporator as a closed-loop flow flash boiling system.

2.1.4 Pulsed flash boiling approach

In a flow flash boiling, the liquid is supplied continuously and at higher heat fluxes a stable vapor film layer could form and the nucleation rate decreases due to lack of liquid surface contact with the evaporator. This will decrease the quality of the liquid-vapor mixture and a long-term dry condition can prevail. To avoid such conditions, a pulsed flash boiling is proposed to interrupt the thermal boundary layer with pulsed flow. The pulsed flashing supplies the liquid methanol to the evaporator for a defined time period in a pulsed flash cycle. During the period where methanol is not supplied, the vacuum pump continuously pumps out the vapor from the low-pressure lines and thus, a higher-pressure gradient is resulted before the start of the next pulse when compared to continuous flow flash boiling. A higher quality of liquid-vapor mixture is also possible while long-term dry-out conditions can be mitigated. To modify the system for performing pulsed flow boiling, a solenoid valve is required between the reservoir and the evaporator as shown in Fig 6. To demonstrate this concept, a closed-loop architecture is developed to form a pulsed flash cooling engineering cycle which is covered in the next section.

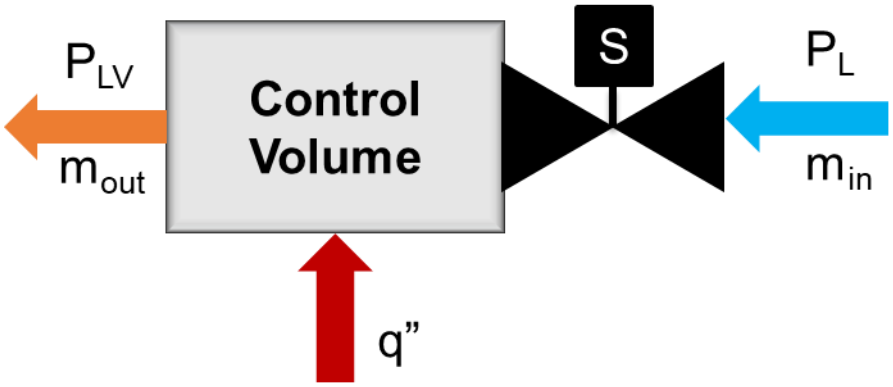

Fig. 6. Required system modification for pulsed flow flash boiling.

2.2. Closed loop flash cooling architecture

The developed closed-loop flash cooling system consists of an evaporator, accumulator, vacuum pump, condenser, and reservoir. The components of a closed loop system are discussed in this section along with sensor details, location, and data acquisition system.

2.2.1. Components of closed loop system

The closed loop flash cooling system with process flow is depicted in Fig 7. The operating fluid employed in the system is methanol whose boiling point is 65 °C. The liquid methanol is pumped from the reservoir using a peristaltic pump and is fed into the evaporator through the solenoid valve. The peristaltic pump can maintain the flow rate from 1-100 ml/min. The reservoir is at atmospheric pressure. The evaporator, accumulator and inlet of the vacuum pump are maintained at a pressure of about 5 kPa before the beginning of the experiment. The outlet of the vacuum pump is a little more or near atmospheric pressure and the condenser extracts the heat from the methanol vapor using a coolant. The condenser used is a coaxial counter flow type, and the coolant used is water at 18 °C. The coolant inlet pressure is at 70 kPa and the outlet pressure is at 40 kPa.

The outlet of the condenser is liquid methanol which is connected to the reservoir. This completes the closed-loop flash cooling cycle.

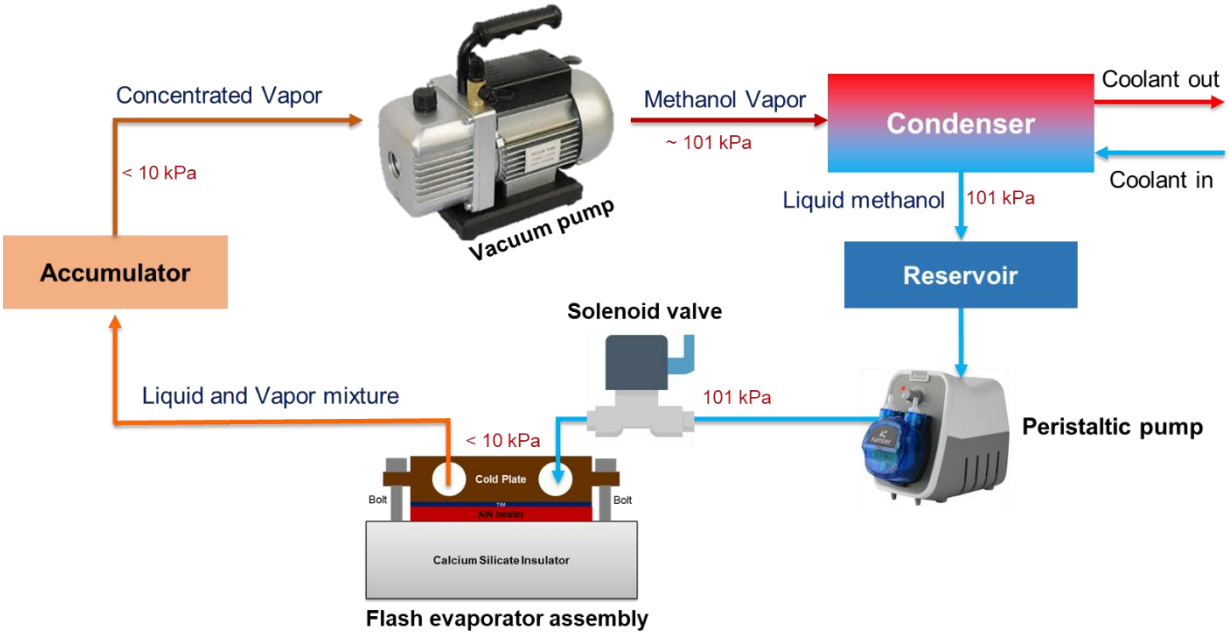

Fig. 7. Closed-loop flash cooling architecture.

Evaporator: The evaporator design can significantly affect the heat extraction performance from the heater. The evaporator dimensions are 25.4 mm x 25.4 mm x 12.6 mm as shown in Fig 8 and are made of copper alloy Cu 110 (99.9% pure copper). It consists of a serpentine channel with 3 turns between inlet and outlet. Each channel is divided into two with a fin extruding from the top sealing plate. This will enable improved contact area between the evaporator and the fluid, increasing the nucleation rates. The top plate is bonded to the bottom evaporator chamber with a gasket in between them. The evaporator was purchased from Custom Thermoelectric [32]. The internal liquid volume is 1.61 ml. The inlet and outlet are 1/16" NPT threaded. The roughness of the evaporator is 0.8 um.

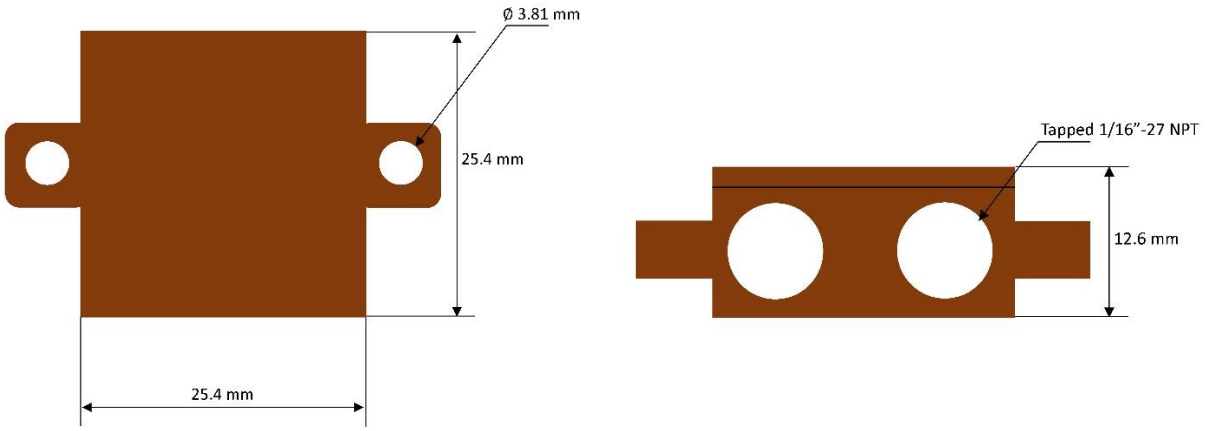

(a) **(b)**

Fig. 8. Schematics of evaporator cold plate (a) top view (b) front view.

Heater: A high heat flux resistive heater is obtained from Watlow which can generate 900 watts of heat. The heating element is covered by Aluminum nitride material. Therefore, the heater does not conduct electricity from its heating element to its surface and the copper surface of the evaporator can be directly mounted. The specification of the heater is described in Table 2.

Table 2. Heater specifications [33]

Heater specifications	
Dimensions	25 mm x 25 mm
Rated Power	900 W
Burn-In Voltage	240 V
Maximum Current (Calculated)	3.75 A
Thermocouple	K type 24 AWG
Maximum operating temperature	400 °C

Nominal resistance at 25 C	64 Ohms
Temperature coefficient of resistivity	0.00150 ± 0.00025 / °C
Roughness	< 1.5 um

Thermal Interface Materials (TIM): A TIM is used to fill the gaps and irregularities between the heating source and the heat sink. In this case, a TIM is applied between the heater and the evaporator. The utilized TIM is OmegaTherm 201, the specifications of which are included in Table 3.

Table 3. Specifications of OmegaTherm 201 [34]

Material	Silicone grease
Maximum continuous operating temperature	200 °C
Cure	Not required
Adhesion	Wets most metal surfaces
Thermal conductivity	2.31 W/mK
Electrical Insulation	Very high

Thermal Insulators: It is desirable to conduct the heat from the heater to the evaporator and not dissipate the heat to the ambient. As the volumetric heat generated in the heater can spread across the entire volume uniformly, insulation is required on the surfaces that do not contact the

evaporator. Three insulators are used including calcium silicate, aerogel and ceramic glass fiber. The aerogel used is made of Pyrogel and its thermal conductivity is 0.023 W/mK at 100 °C [35]. Aerogel is primarily a porous substrate with a higher volume of air which could provide a cushioning effect for the heater to withstand sufficient compressive load provided by bolts. The maximum operating temperature is 650 °C. Calcium silicate is one of the furnace materials, and it is machined to a dimension of nearly 50 mm x 100 mm with a thickness of 25.4 mm (1”). It has an R-value of 1.3 and the maximum operating temperature is 926 °C [36]. It is used to mount the evaporator using bolts. In other words, calcium silicate acts as a substrate to hold the evaporator as well as an insulator. Ceramic glass fiber is a commonly used insulator and is employed to cover the side wall and other surfaces of evaporator that are exposed to ambient air.

Evaporator assembly: The evaporator assembly consists of an evaporator, TIM, heater, aerogel, and calcium silicate insulator stacked upon one other. A uniform TIM layer is applied on the top surface of the heater and the evaporator is pressed against the TIM. The bottom side of the heater is stacked on the aerogel layers which in turn is stacked upon calcium silicate insulator. Two bolts run through the bolt holes and are twisted enough to provide sufficient pressure to hold the evaporator assembly. The position of the hex nuts is carefully chosen to align with the bolt hole of the evaporator. The calcium silicate insulator is drilled, and the hex nuts are placed deep into the insulator. Thus, the bolt goes all the way inside the calcium silicate insulator. The bolt is made of stainless steel. The schematics and the experimental image of the evaporator assembly are depicted in Fig 9.

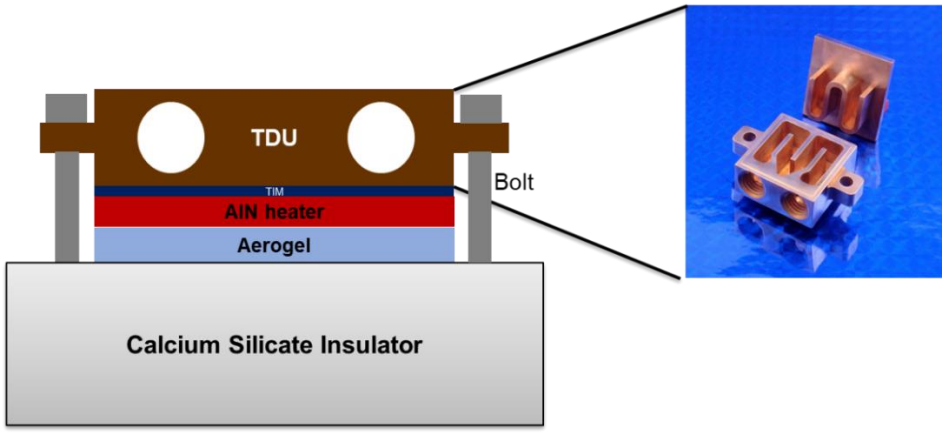

(a)

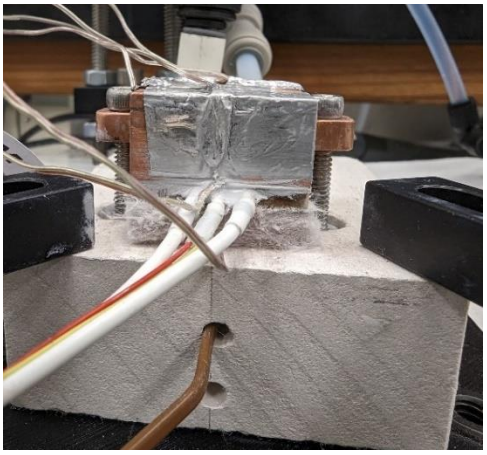

(b)

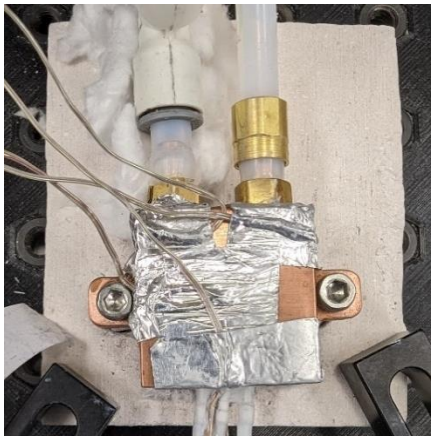

(c)

Fig. 9. Evaporator assembly (a) schematics (b) experimental image rear view (c) experimental image top view.

Accumulator: This container has a 3-gallon capacity, and the inner diameter and height are 9" and 17.4", respectively. It is made to operate at vacuum pressure. The prime function of the accumulator is to separate the liquid from the liquid-vapor mixture coming from the evaporator. All the ports (four) of the accumulator are present at the top and only one port has a pipe that goes all the way down the accumulator to be base. This port is marked as an inlet of the accumulator

which is connected to the outlet of the evaporator. The other port of the accumulator is regarded as the outlet which is connected to the vacuum pump. Here, the liquid vapor mixture is pushed down the pipe inside the accumulator and the vapor rises to the top while the liquid accumulates at the bottom due to the action of gravity. The vacuum pump will pull the rising vapor and thus, concentrated vapor enters the vacuum pump. It is important to operate the vacuum pump with as much vapor as possible to maintain its longevity and efficiency. The experimental setup of the accumulator and vacuum pump is represented in Fig 10.

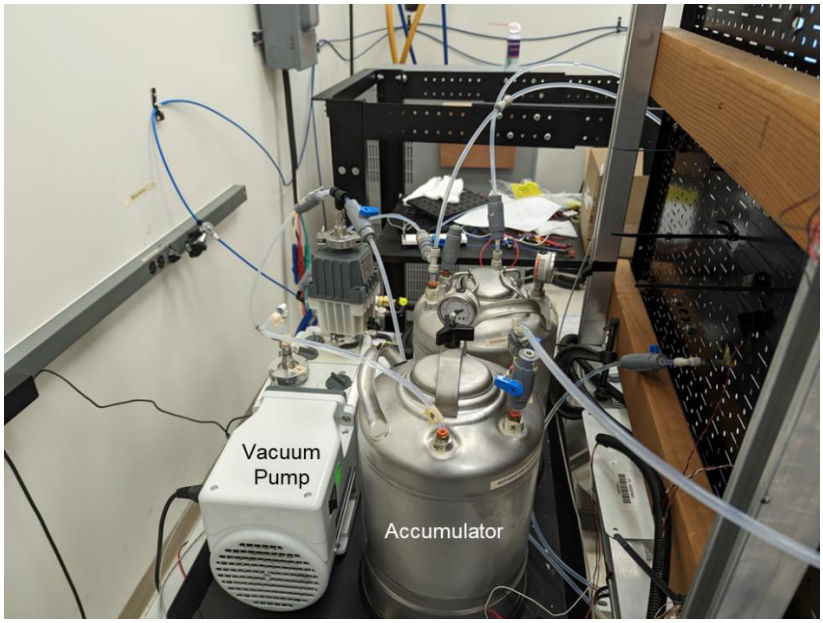

Fig. 10. Experimental setup of Accumulator and Vacuum pump.

Vacuum pump: A rotary vane oil-sealed vacuum pump (Edward RV3) is used. The specification of the vacuum pump is detailed in Table 4. The vacuum pump is also fitted with an oil mist filter.

Table 4. Vacuum pump specifications [37]

Maximum displacement	4.5 m^3/hr

Maximum pumping speed	3.9 m^3/hr
Maximum outlet pressure	0.2 bar gauge
Maximum oil capacity	0.7 L
Minimum oil capacity	0.42 L
Pump power	550 W
Motor rotational speed	1760 rev/min

Condenser: The condenser used is of coaxial counterflow type. The refrigerant loop of the condenser is connected to the methanol line. The inlet of the refrigerant line of the condenser is connected to the outlet of the pump and the outlet of the refrigerant line of the condenser is connected to the inlet of the reservoir. The coolant loop of the condenser is connected to the building water supply of the laboratory. The supply and return pressure of the building water supply is 70 psi and 40 psi, respectively. This pressure difference is sufficient to drive the coolant water across the condenser. The building water supply temperature is monitored for a complete day and the temperature stays nearly stable around 18 °C. The target condenser outlet temperature of methanol is room temperature which is ~20 °C. The flow rate and the lower temperature of the coolant were sufficient to cool the vapor from saturation state to room temperature. It is also important to note that the length of the condenser is long such that maximum heat rejection is achieved in the condenser. The specification of the condenser is included in Table 5 and the condenser is shown in Fig 11.

Table 5. Specifications of condenser [38]

Refrigerant Inlet connection	3/8” (OD)
Refrigerant Outlet connection	3/8” (OD)
Water inlet connection	5/8” (OD)
Water outlet connection	5/8” (OD)
Maximum refrigerant working pressure	650 psi
Maximum water working pressure	500 psi
Capacity	2 ton
Outer shell	Carbon Steel
Inner Tube	Copper

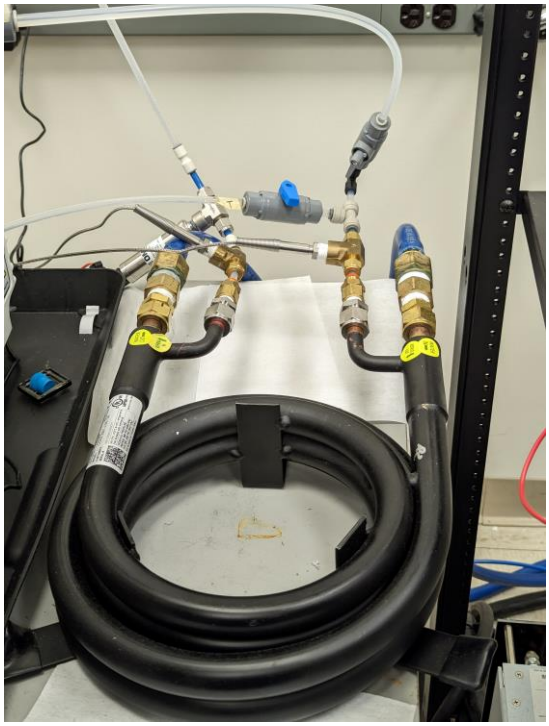

Fig. 11. Counter flow coaxial condenser.

Reservoir: The reservoir is also a container similar to the accumulator with four ports. The only difference is that the lid of the reservoir is made for handling high pressures while the accumulator's lid is made to withstand primarily the vacuum pressure. One of the four ports has a pipe running from the top to the bottom of the reservoir which is regarded as an outlet. The methanol is pumped out to the evaporator using this outlet port through the peristaltic pump. One port is used as an inlet and another port is used to measure gauge pressure. The remaining port is connected to a ball valve such that it can be switched on and off to release the pressure if required.

Peristaltic pump: A peristaltic pump is a type of positive displacement pump that works on the principle of peristalsis, which is the wave-like contraction and relaxation of muscles. In a peristaltic pump, a flexible tube is squeezed or compressed by a set of rollers that move along the tube. This action propels the fluid through the tube in a pulsatile manner. A low flow rate peristaltic pump is used where the flow rate can be varied from 1 to 100 ml/min. The pressure exerted by the peristaltic pump is very low. This pump has bidirectional flow features and can also be calibrated when required.

Solenoid valve: A 2-way normally closed solenoid valve is used. The specifications of the solenoid valve are shown in Table 6

Table 6. Solenoid valve specifications [39]

Pipe size	¼" NPT
Operating pressure	0-1300 psi
Flow coefficient	0.07 Cv
Operation	2-way, normally closed solenoid valve
Vacuum rating	0.001 Torr

Body material	Brass
Seal	PTFE
Power	8 W
Voltage	12 V
Duty cycle	Continuous, 100% ED

Power supply: The power supply used is a 25 kW Magna DC programmable power supply. The specifications are detailed in Table 7. Furthermore, the power supply is equipped with a High Slew Rate Output (+HS) which enables the power supply to operate as a low-frequency power pulse generator and solves limitations inherent in switching power supply design. It is also equipped with the LXI TCP/IP Ethernet (+LXI) option. This option allows the power supply to be fully controlled over an integrated TCP/IP Ethernet interface using Python, MATLAB, C and C#. Moreover, it is NI LabVIEW supported.

Table 7. Specifications and features of DC power supply [40]

Maximum DC voltage	500 V
Maximum DC current	50 A
Maximum power	25 kW
Load transient response	2 ms to recover within ±1% of regulated output with a 50% to 100% or 100% to 50% step load change
Measurement accuracy	Voltage: ±0.2% of max voltage rating Current: ±0.2% of max current rating

Maximum Slew rate	4 ms, output voltage change from 0 to 63% 8 ms, output current change from 0 to 63%
Computer command protocol	Standard Commands for Programmable Instruments (SCPI)

Piping: A semi-clear Teflon PTFE pipe is used throughout the closed-loop flash cooling system. The inner and outer diameter of the pipe are 1/8" and 1/4", respectively. These are semi-flexible pipes with a bend radius of 1 ½". The operating temperature range varies from -450 °F to 500 °F and the maximum pressure rating is 300 psi at 72 °F.

2.2.2. Measurement and data acquisition system

As flash cooling deals with boiling phenomena driven by pressure, it is important to measure both temperature and pressure in the system. Thermocouples are used to measure the temperature, and pressure transducers are employed to measure the vacuum pressure. All thermocouple and pressure transducer data are collected using the National Instruments Data Acquisition (NI DAQ) system and are interpreted as well as stored using LabVIEW software.

Thermocouples: Thermocouple works on the Seebeck effect where the temperature difference between the junction materials produces a voltage difference. This voltage is measured as a function of temperature and is read in LabVIEW. Overall, eight thermocouples are located in the flash cooling circuit, and all thermocouples are K-type. The measured temperature location includes fluid inlet, evaporator inlet wall, evaporator rear wall, evaporator outlet wall, heater, fluid outlet, condenser inlet and condenser outlet. All three evaporator wall thermocouple beads are

positioned in a way that they contact the bottommost surface of the wall, near the heat source. All the thermocouples have been calibrated by the seller.

Pressure transducers: The pressure transducer used converts the pressure force to electrical signals which are read by the DAQ system. A flexible diaphragm is employed to convert the pressure force of the fluid to a change in electrical current using a strain gauge. A vacuum pressure transducer outputs 4-20 mA where 20 mA corresponds to ~0 psi. Two vacuum pressure transducers and one gauge pressure transducer are used. The former is employed in between the accumulator and the evaporator outlet while the latter is employed between the condenser inlet and the vacuum pump outlet. The pressure sensors were calibrated by the manufacturer where the pressure values in the calibration sheet are cross verified for atmospheric pressure and 7.5 vacuum gauge psi before executing the designed experimental matrix.

NI DAQ: The compact DAQ system houses 1 thermocouple module, 1 current input module and 1 relay module. The thermocouple module (NI 9212) consists of 8 channels and can acquire data at 95 Hz at each channel. The current input module measures the current signals from the pressure transducer. The data is acquired at 10 Hz to capture the oscillation in each pulse cycle time. The relay module controls the solenoid valve enabling the pulse mechanism. The power supply to the solenoid valve is connected through a relay module.

LabVIEW software: LabVIEW software is used to collect, analyze and command actuators involved in the flash cooling system. The graphically coded LabVIEW user interface page is depicted in Fig 12. The main coded features include PID control for the heater, data acquisition, data storing, safety controls, solenoid valve control and power supply integration. PID control for the power supply is used to maintain constant power input in case the resistance of the heater changes due to its temperature. Data is stored in the Excel format which is later post-processed.

The coded safety features include over-voltage protection, over-current protection, system operating temperature protection and heater protection.

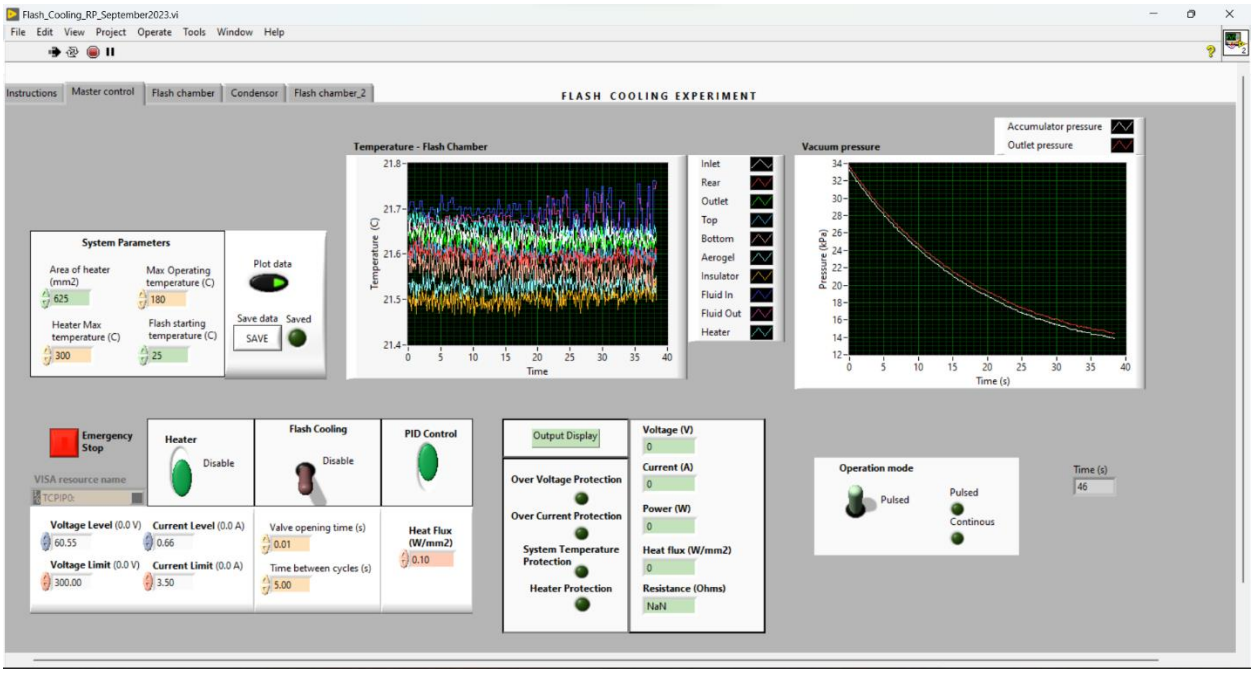

Fig. 12. LabVIEW interface.

Measurement uncertainty: The employed sensors include eight thermocouples and three pressure transducers that measure temperature and pressure. The uncertainty in the standard K-type thermocouple is ± 2.2 °C. The uncertainty in the pressure transducer is 0.08 %.

2.3. Design of Experiments (DoE)

In the proposed closed-loop flash cooling system, three control parameters influence the performance of the system. These include applied heat flux (or heat input), flow rate and pulse cycle time. The flow rate in this system is defined as the ratio of the volume of methanol per pulse

to the pulse cycle time. Therefore, the flow rate is a time-averaged flow rate. Pulse cycle time on the other hand is a summation of the active (t_{ON}) and dormant (t_{OFF}) duration of the solenoid valve.

The experiments aim to understand the system and find meaningful observations that help in mapping the feasible operating conditions of the flash cooling system. Experiments were conducted by varying heat flux from 0.2 to 1 W/mm^2, which corresponds to a heat input range of 125 W to 625 W, respectively. The design of experiment for a given heat flux is varied with the pulse cycle time to determine the optimal cooling conditions. In the preliminary experiments, the peristaltic pump and its associated hydraulic circuit were not installed. Thus, the flow rate is measured by using a syringe. A known volume (50cc) is filled into the syringe and the connection from the reservoir to the evaporator is shut off. This is to ensure that the evaporator consumes the liquid mass only from the syringe. During experimentation, the time taken to consume a predefined amount of methanol (2 ml for a low flow rate and 5 ml for a high flow rate) is noted down and averaged for the entire volume of the syringe to determine the time-averaged flow rate. Once all the methanol in the syringe is about to be consumed, the valve is turned on for a continuous supply of methanol. It is noteworthy that the liquid methanol is consumed by the evaporator only due to the pressure gradient between the evaporator pressure and the liquid at atmospheric pressure.

A direct way of controlling the flow rate accurately is not possible since it depends on the pressure difference between the upstream and downstream lines of the solenoid valve. Therefore, the flow rate is controlled by the solenoid valve timings or pulse cycle time. Two ways are possible to achieve the same flow rate. One way is to increase t_{ON} time for each cycle time and reduce the pulse frequency and another approach is to provide shorter t_{ON} time for each cycle time and increase the pulse frequency. The preliminary experiments will aid in understanding the correlation between the pulse cycle time or pulse frequency and the flow rate. With the previous sample

experiments and collected data, it is possible to estimate the t_{ON} and t_{OFF} conditions to provide a desired flow rate to the system. However, the main constraint of choosing a flow rate is that the latent heat of the supplied mass of methanol should be greater than the heat input ($\dot{m}h_{fg} > q$). This is to ensure that the steady periodic condition can be achieved, or else the system's temperature will not stabilize (sensible heat is neglected since the superheated conditions prevail inside the evaporator).

Initially, the experiment is run and monitored until steady periodic conditions are reached. A steady periodic condition means that the oscillation in each measured quantity remains stable with time for several pulse cycles. A steady periodic condition for temperature and pressure is determined when it exhibits stable maximum and minimum values across pulse cycles. A steady periodic condition is achieved when outlet pressure, evaporator inlet, rear, and outlet wall temperature, and fluid outlet temperature have stable oscillations. In the case where the steady periodic condition is not achieved, t_{ON} time is increased for the next experiment with the same heat flux. Pulse cycle time is reduced by reducing t_{OFF} time if steady periodic conditions are not achieved even after increasing t_{ON} time. The overall objective of this design of experiments is to have at least one experiment achieving steady-periodic conditions for each considered heat flux. On the other hand, if the steady-periodic condition is achieved with the first set of input parameters for a given heat flux, then the subsequent experiment is performed by reducing t_{ON} to analyze the influence of increasing flow rate. Furthermore, if increasing t_{ON} does not yield much difference in the performance, t_{OFF} is decreased to reduce the pulse cycle time.

Chapter 3. Results and discussion

3.1. Experimental results

Each experiment is performed for 1800 seconds to ensure that the temperature of the evaporator and outlet pressure of the evaporator achieve nearly steady periodic conditions. The change in pressure oscillations is highly sensitive to the operating pulse timings. An experimental time of 1800 seconds was sufficient to witness stable oscillations for each heat flux. The results of the 23 experiments are summarized in Table 8.

Sample temperature and pressure profiles corresponding to lower heat flux (higher pulse time) and higher heat flux (lower pulse cycle time) are shown in Figs 13 and 14. In any experiment, the flash cycle starts only when the average evaporator temperature reaches greater than 40 °C before which the evaporator is subjected to only heating. Constant heat flux is maintained with the assistance of PID control. The PID control essentially accommodates any variations in the resistance of the heating element such that constant power is maintained. The PID required around an initial 6-12 seconds (depending on heat flux value) to achieve the targeted heat flux, and the evaporator is not subjected to constant heat flux conditions during this initial time range. The temperature and pressure oscillate and rise gradually toward steady periodic conditions after 1200 seconds as indicated by repeating oscillations within a stable range. The evaporator design consists of a serpentine pattern. Therefore, the outlet wall temperature is expected to be greater than the rear wall and inlet wall temperature. However, the oscillations observed in each of these three temperatures in the evaporator are in phase.

Table 8. Summary of 23 experiments.

Experiment number	Heat flux	Power	Solenoid valve		Pulse cycle time	Flow rate	Volume per pulse	Temperature				Outlet Pressure
			t_{OFF}	t_{ON}				Average Evaporator wall	Heater	Fluid Inlet	Fluid Outlet	
	W/mm^2	W	s	s	s	ml/s	ml	˚C	˚C	˚C	˚C	kPa
1	0.2	124.71	5	0.06	5.06	0.137	0.687	53.34	73.37	22.76	27.27	17.96
2	0.2	124.71	5	0.05	5.05	0.118	0.591	Insufficient flow rate / cooling				
3	0.2	124.58	5	0.07	5.07	0.157	0.783	45.26	65.01	22.49	26.93	18.04
4	0.3	186.99	5	0.1	5.1	0.222	1.108	55.01	84.95	21.36	24.44	15.13
5	0.3	187.14	5	0.11	5.11	0.236	1.178	67.91	99.03	23.30	33.63	24.60
6	0.3	187.93	4.5	0.1	4.6	0.239	1.075	59.70	90.04	22.77	24.81	14.94
7	0.4	251.14	4	0.11	4.11	0.287	1.148	81.30	126.00	22.91	39.24	31.45
8	0.4	250.24	4	0.13	4.13	0.342	1.367	80.51	125.68	23.70	39.35	32.14
9	0.4	251.14	3	0.11	3.11	0.373	1.119	72.79	117.12	24.14	38.84	31.85
10	0.5	311.42	3	0.13	3.13	0.404	1.213	The system temperature limit has been reached				

11	0.5	310.64	3	0.15	3.15	0.452	1.357	The system temperature limit has been reached				
12	0.5	312.64	2	0.08	2.08	0.397	0.794	79.97	138.79	25.37	43.17	39.45
13	0.6	375.16	1.5	0.08	1.58	0.498	0.748	The System temperature limit has been reached				
14	0.6	375.16	1.5	0.1	1.6	0.603	0.904	88.11	163.75	26.22	46.75	46.56
15	0.6	375.16	1	0.06	1.06	0.629	0.629	84.95	161.05	25.86	46.58	46.73
16	0.7	437.35	1	0.06	1.06	0.583	0.583	Insufficient information				
17	0.8	498.87	1	0.08	1.08	0.676	0.676	The system temperature limit has been reached				
18	0.8	495.75	0.8	0.05	0.85	0.603	0.483	The system temperature limit has been reached				
19	0.8	499.85	0.6	0.05	0.65	0.798	0.479	96.68	169.42	24.75	55.45	60.32
20	1	626.20	0.4	0.05	0.45	1.036	0.415	The system temperature limit has been reached				
21	1	624.89	0.3	0.03	0.33	0.894	0.268	The system temperature limit has been reached				
22	1	624.89	0.3	0.04	0.34	1.039	0.312	The system temperature limit has been reached				
23	1	625.68	0.25	0.03	0.28	0.985	0.246	114.21	211.75	24.10	60.33	74.97

It is important to note that the TIM material also imparts thermal resistance which plays a crucial role in a huge thermal gradient across the heater and the evaporator. As the evaporator is insulated with calcium silicate and ceramic glass fiber insulators, the heat lost by convection is minimized. The inlet temperature is maintained in the range of 21 – 25 °C which is equivalent to the condenser outlet temperature. The temperature of the evaporator stabilizes after 1200 seconds while the outlet pressure stabilizes after 1400 seconds across all experiments. Therefore, an experiment time of 1800 seconds will be sufficient to capture the steady-periodic conditions.

In the temperature profile, there are instances where a sudden deviation in the curve is observed. This region corresponds to the scenario where non-condensable gases come in contact with the evaporator wall. These non-condensable gases hinder the heat transfer, and the temperature of the evaporator wall shoots up. However, as and when the methanol comes in contact with the evaporator wall, the temperature is stabilized within the typical temperature profile. In Fig 13(a), the sudden peak in temperature around 1000 seconds is an example of the system's recovery even after encountering a non-condensable gas bubble. In the pressure plot, the effect is reflected as sudden higher oscillations and gradually the oscillations are brought back to the range it was oscillating before encountering gas bubble. It is noteworthy that a considerable amount of gas bubble can raise the wall superheat such that the film boiling is favored, and the steady periodic condition cannot be achieved. This is especially true for high heat flux and the highest feasible pulse cycle time conditions.

(a)

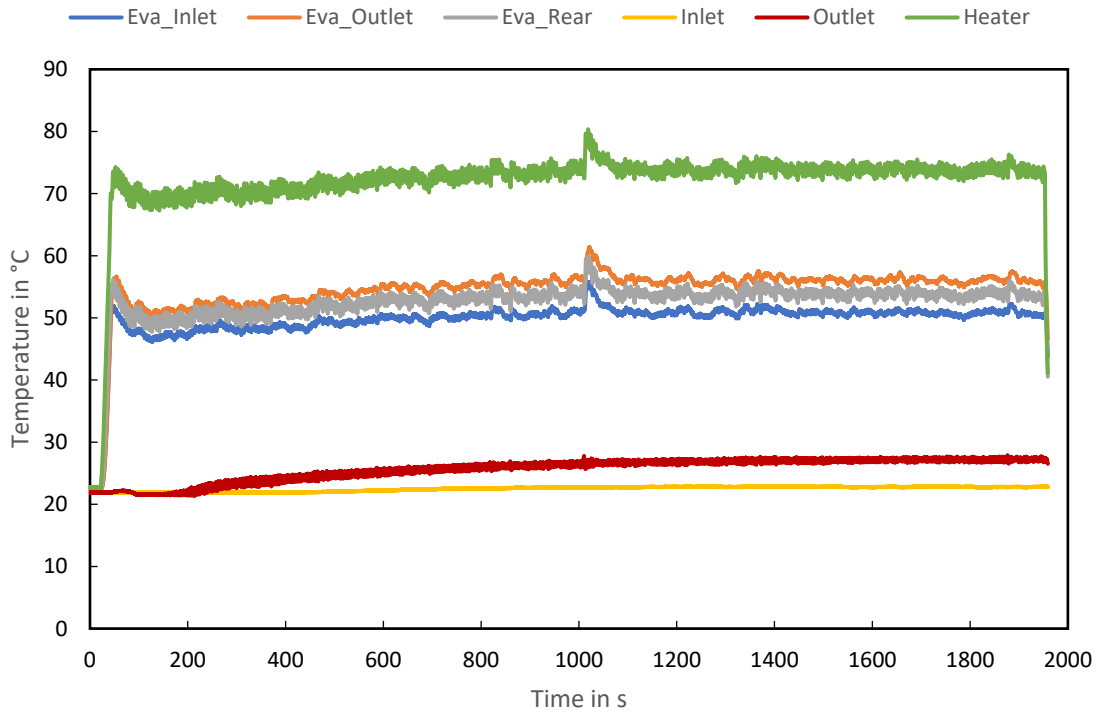

(b)

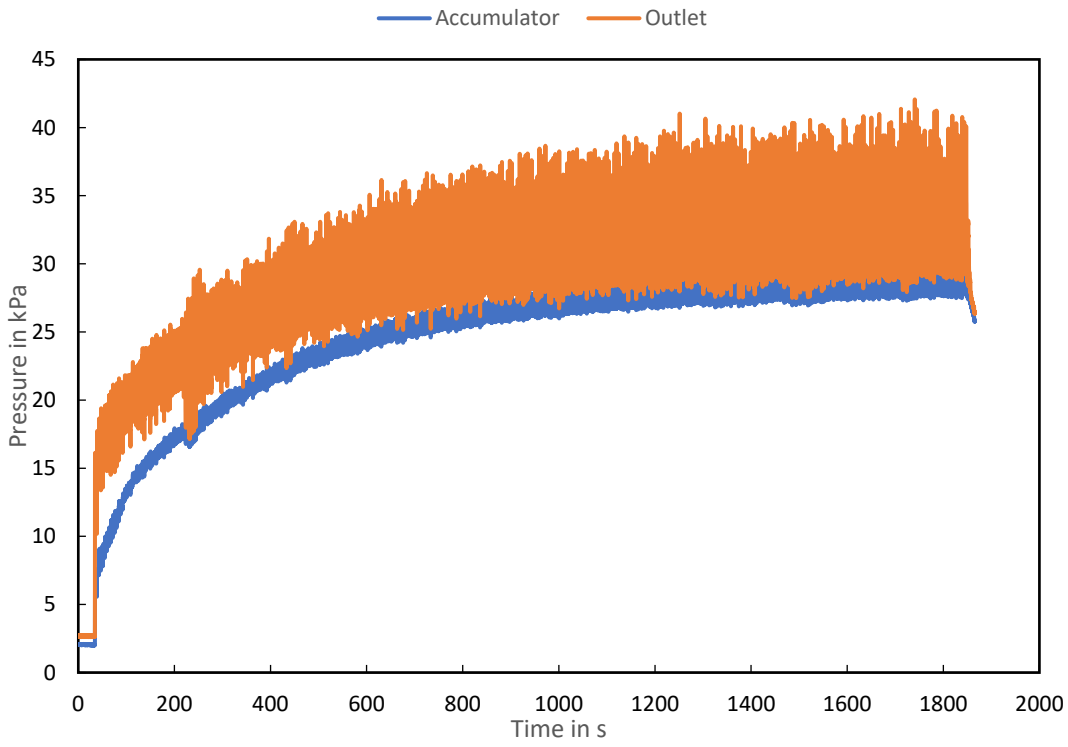

Fig. 13. (a) Temperature profile (b) Pressure profile for a heat flux of 0.2 W/mm^2, 5 seconds pulse cycle time and 0.137 ml/s flow rate.

(a)

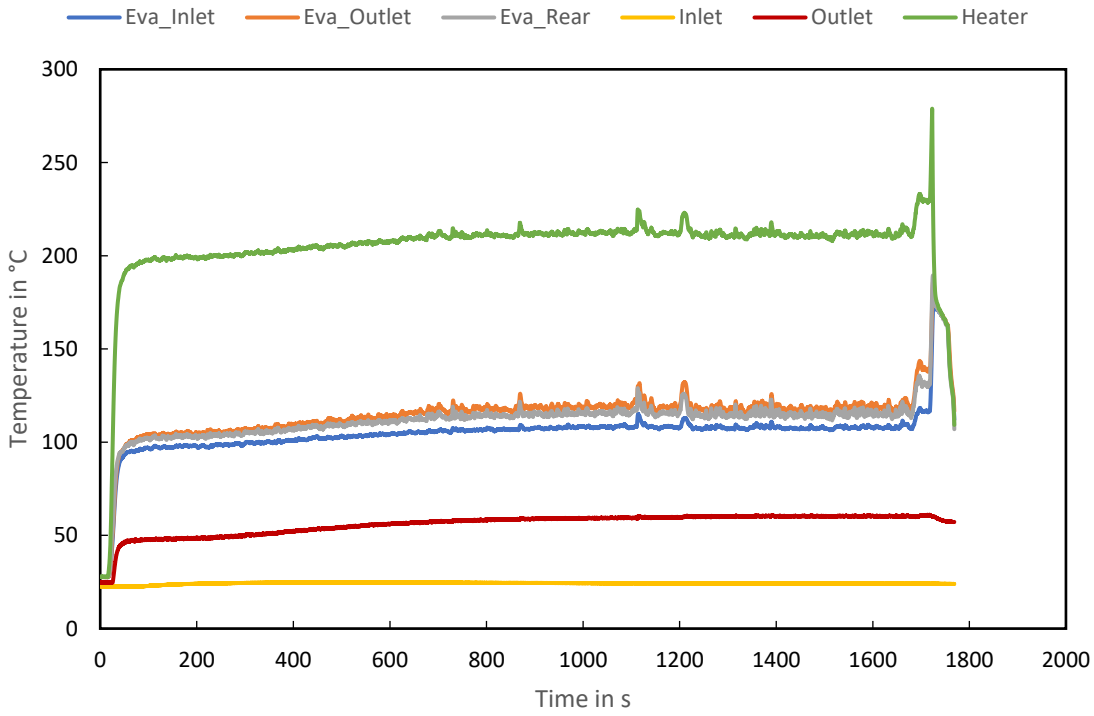

(b)

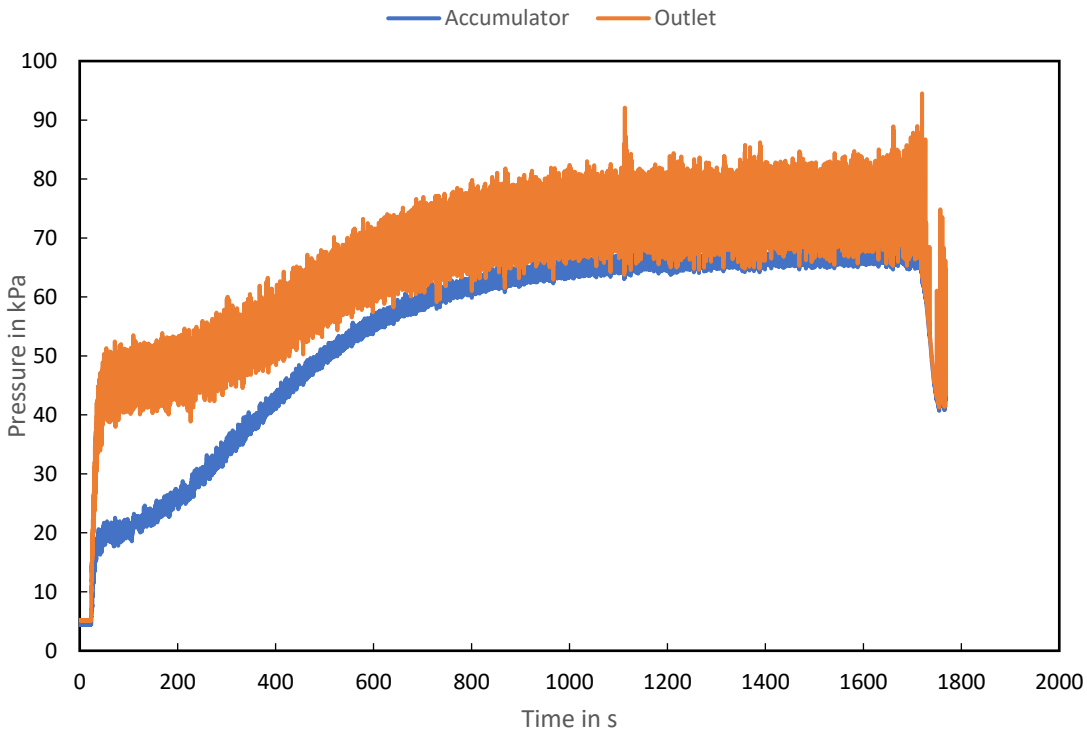

Fig. 14. (a) Temperature profile (b) Pressure profile for a heat flux of 1 W/mm^2, 0.28 seconds pulse cycle time and 0.985 ml/s flow rate.

The average steady periodic temperature of the evaporator is within 85 °C for heat fluxes ranging from 0.2 to 0.6 W/mm^2. Although the average temperature of the evaporator is higher than 85 °C for heat fluxes 0.8 W/mm^2 and 1 W/mm^2, it is interesting to observe the necessary conditions to achieve steady periodicity for such high heat fluxes. There are experimental cases where the system temperature limit is reached, meaning that the experiment is halted for safety reasons as the temperature was continuously rising. The system temperature limit was 120 °C for heat fluxes ranging from 0.2 to 0.6 W/mm^2 and it is 150 °C for high heat fluxes ranging from 0.8 to 1 W/mm^2.

3.2. Heat loss estimation

The heat loss from the evaporator assembly can be determined as a product of thermal conductance and temperature difference between the evaporator and the ambient. The effective surface area exposed to ambience before insulation is 1875 mm^2. The heat transfer coefficient for free convection in air is in the range of 10 W/m^{2}K and ambient temperature is 20 °C. The estimated heat loss from convection and radiation to the ambient is 10.4 W for 1 W/mm^2 heat flux. The estimated conduction loss to the aerogel is estimated to be 0.079 W. In the experimental system, the major loss is accounted as conductive heat loss in TIM. The heat loss across the TIM and the bottom surface of copper cold plate ranges from 14 W to 87 W corresponding to the heat fluxes 0.2 W/mm^2 (125 W) and 1 W/mm^2 (625 W), respectively. In summary, heat loss occurs in aerogel and TIM as conductive heat loss, the rest is accounted for convective and radiation heat losses from evaporator assembly to the ambient. The convective and radiative heat losses from Calcium silicate insulator to the ambient is neglected.

3.3. The role of pulse cycle time

One of the key findings is that the pulse cycle time is the dominant control parameter that affects the performance of the system. For instance, in experimental cases 5 and 6, the system is subjected to a heat flux of 0.3 W/mm^2, and the time-averaged flow rate is almost the same with a difference of 0.003 ml/s. The only varying parameter is the pulse cycle times which were 5.11 and 4.6 seconds for experimental case 5 and 6, respectively. The results indicate that the average steady periodic temperature of case 6 was 8.2 °C lower than case 5. Similarly, for 0.5 W/mm^2, the average steady periodic temperature was 78 °C for case 12 with 2.08 seconds of pulse cycle time. On the other hand, case 11 with the same heat flux but a pulse cycle time of 3.15 seconds reaches the allowable system temperature limit. Another relevant observation is that the flow rate of case 11 is 0.05 ml/s higher than that of case 12. Thus, even if a higher flow rate is supplied and if the pulse frequency is not high enough, the system does not achieve steady periodic conditions. Similar observations are found for 1 W/mm^2 when comparing cases 22 and 23. Altogether, the pulse cycle time is clearly the dominant control parameter; lower pulse cycle times produce better cooling.

The foregoing observation suggests a physical hypothesis.. Pulsed flashing supplies methanol only for a fraction of the pulse cycle time. During the time duration for which the methanol is not supplied, the evaporator is subjected to only heating, neglecting residual methanol in the evaporator. This condition increases the wall superheat and when the liquid is supplied to the evaporator in the next cycle, the heat from the wall is removed and again the wall superheat decreases. Therefore, an oscillation occurs in the wall superheat in each pulse cycle. The longer the pulse cycle time (lower frequency), the higher the degree of oscillations. When operating at higher heat fluxes, the higher oscillations can raise the wall superheat to a value where conditions to form a stable vapor film is favored to hinder the heat transfer from the evaporator wall, raising

the temperature of the evaporator rapidly and further raising the wall superheat. Eventually maximum allowable system operating temperature is reached, and the power supply to the heater is terminated for safety. Hence, the pulse frequency controls the oscillations in the wall superheat. The lower the pulse cycle time, the smaller the oscillations. At a high heat flux of 1 W/mm^2, even a short pulse cycle time of 0.45 seconds is not sufficient to hinder the formation of vapor film as can be observed in case 20 from Table 8. These results indicate that the highest feasible pulse cycle time is highly sensitive to the applied heat flux, and it can be as low as 0.28 seconds for 1 W/mm^2.

In a pulse cycle, if t_{ON} time increase, then the volume per pulse cycle increases to produce higher time-averaged flow rate. For a given heat flux, the goal of the design of the experiment is to identify a feasible t_{ON} and t_{OFF} to achieve steady periodic conditions. Once a feasible pulse cycle time is determined, t_{ON} is increased in the successive experiment by maintaining t_{OFF} as a constant to assess its influence on the steady-periodic temperature. In terms of pulse cycle time, increasing t_{ON} alone increases the pulse cycle time, and resulting in a reduced steady periodic temperature due to increased flow rate. Experimental cases 7 and 8 serve as examples of the above-discussed phenomenon. The key observation is that better performance is achieved despite increasing the pulse cycle time. Nevertheless, the increase in pulse cycle time is in the range of 10 ms. At a moderate heat flux of 0.5 W/mm^2, the increase in t_{ON} by maintaining t_{OFF} as constant does not aid in achieving steady periodic conditions and the dominance of pulse cycle time is clear from 0.5 W/mm^2 to 1 W/mm^2. Increasing t_{ON} in a pulse cycle time by maintaining t_{OFF} as constant can be related to the duty cycle expressed as a percentage. The higher the duty cycle of the solenoid valve, the higher the flow rate.

3.4. Outlet pressure

The outlet pressure represents the pressure of the liquid-vapor mixture emerging from the evaporator. In the flash cooling system, outlet pressure can be regarded as a function of flow rate and outlet fluid temperature. As predicted, the outlet pressure increases with temperature and flow rate. According to the outlet temperature, the outlet pressure increases by following the Clausius–Clapeyron relation as represented by the orange line in Fig 15, which also serves as an evidence that the outlet methanol is in saturation conditions and boiling occurs. The variation in outlet pressure as a function of flow rate follows a linear trend as shown in Fig 16.

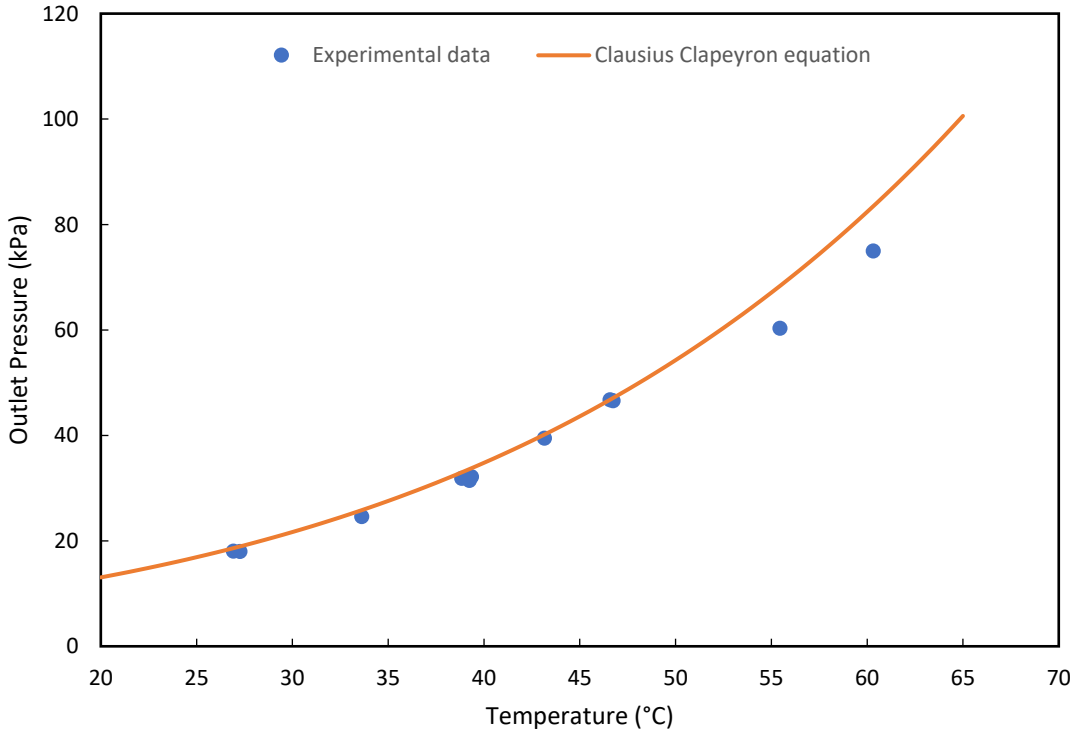

Fig. 15. Outlet pressure vs Outlet temperature plotted with Clausius Clapeyron equation.

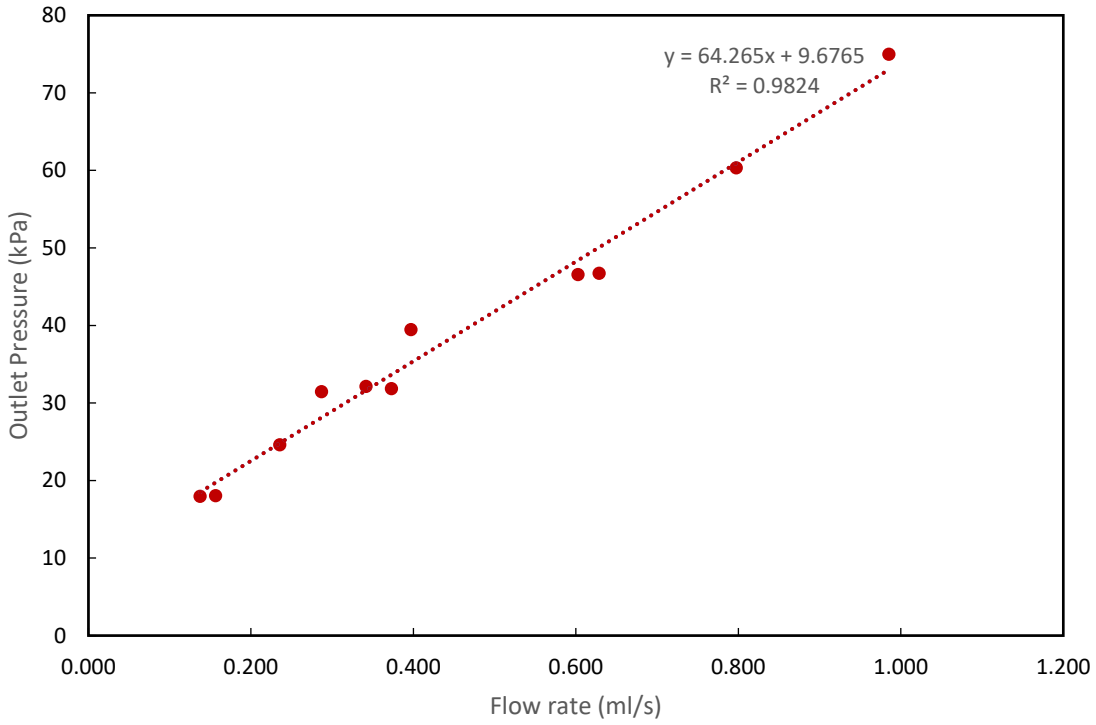

Fig. 16. Outlet pressure vs flow rate.

3.5. Oscillation characteristics

Oscillations in temperature and pressure are attributed to pulsed flashing, and local oscillations occur due to nucleation. With regards to the temperature profile, the oscillations are larger for (i) higher pulse cycle time irrespective of flow rate and heat flux, (ii) higher heat fluxes for a given pulse cycle time and (iii) lower flow rate for a given heat flux and cycle time. Maximum and minimum oscillations in temperature and outlet pressure are shown in Figs 17-20. Table 9 represents the oscillations in the best-case results of each heat flux. It can be observed that a maximum oscillation in temperature is about ± 3.5 °C and maximum pressure oscillations are around ± 9 kPa for a heat flux of 1 W/mm^2, pulse cycle time of 0.28 seconds and a flow rate of 0.98 ml/s. Although the pulse cycle time is shorter, it produced higher oscillations because the

pulse cycle time was closer to the minimum feasible pulse cycle time, or the conditions observed are near to quasi-steady state.

Table 9. Oscillations in temperature and pressure for best experimental results for each heat flux.

Experiment number	**Heat flux in W/mm^2**	**Oscillations in evaporator temperature**	**Oscillations in outlet Pressure**
3	0.2	± 1 °C	± 1.5 kPa
9	0.4	± 1.5 °C	± 3 kPa
12	0.5	± 1.5 °C	± 4.5 kPa
15	0.6	± 0.6 °C	± 3.5 kPa
19	0.8	± 1.5 °C	± 5.5 kPa
23	1	± 3.5 °C	± 9 kPa

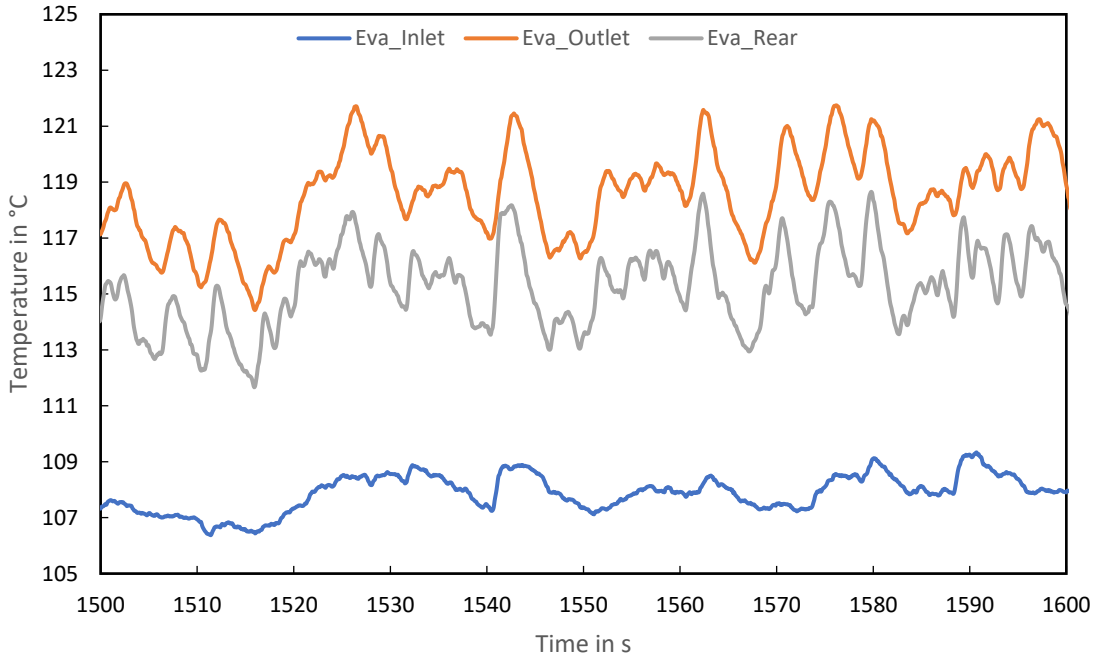

Fig. 17. Maximum steady-periodic oscillation in temperature corresponding to 1 W/mm^2.

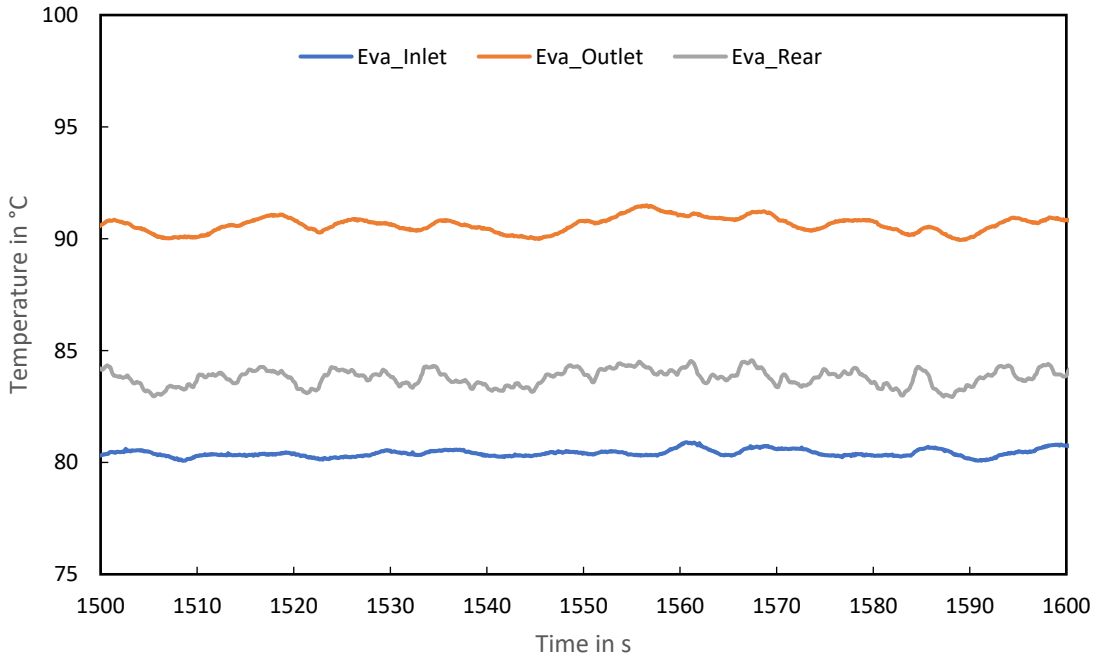

Fig. 18. Minimum steady periodic oscillations in temperature corresponding to 0.6 W/mm^2.

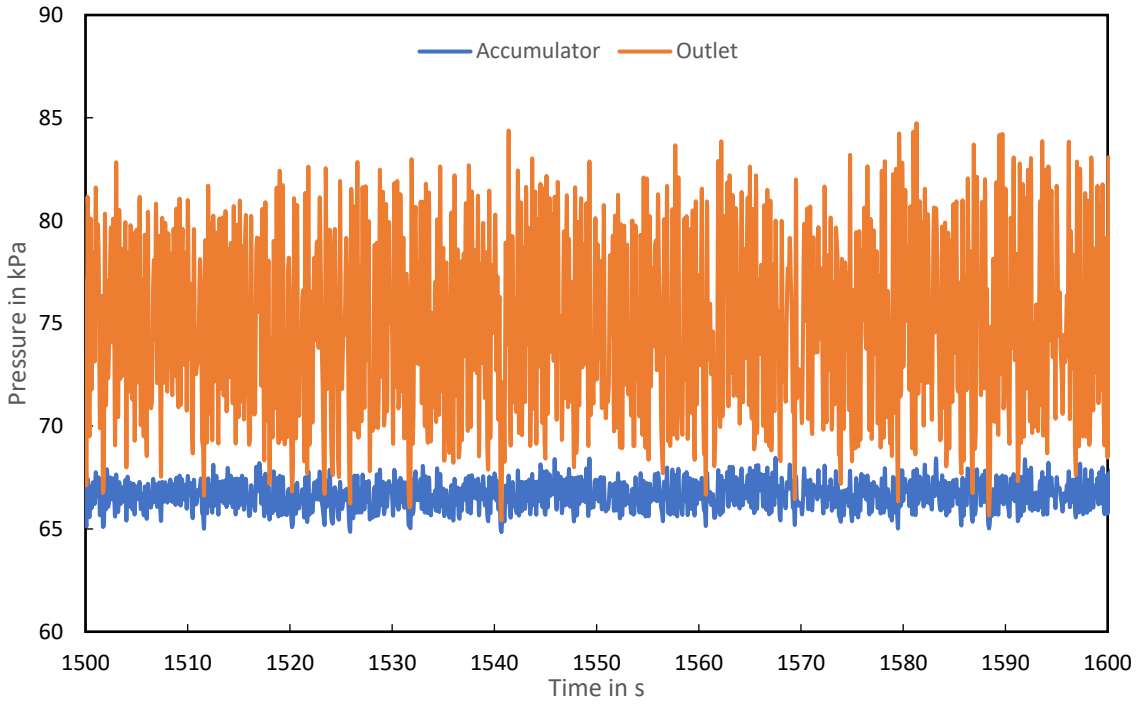

Fig. 19. Maximum steady periodic oscillation in outlet pressure corresponding to 1 W/mm^2.

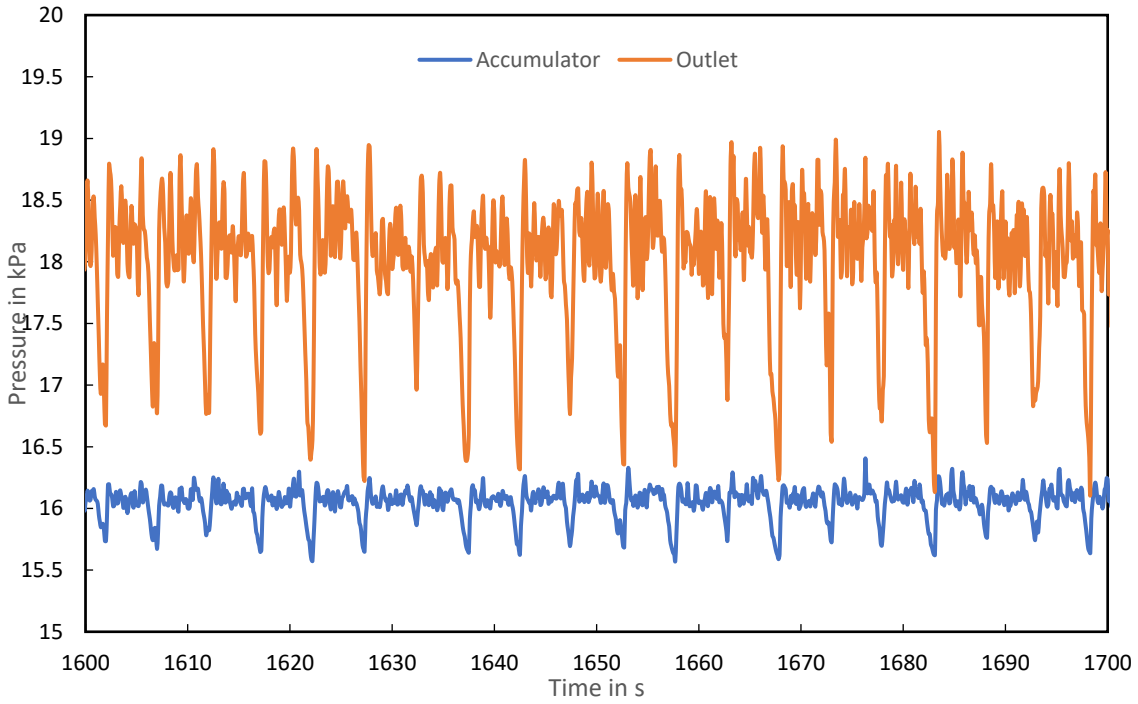

Fig. 20. Minimum steady periodic oscillations in outlet pressure corresponding to 0.2 W/mm^2.

3.6. Thermal resistance

Thermal resistance would yield a normalized approach to measure the performance of the evaporator. The thermal resistance is calculated by using Eqs. (2) and (3).

$$\Delta T = T_{evaporator} - 0.5 * (T_{m,i} + T_{m,o}) \tag{2}$$

$$R_{th} = \frac{\Delta T}{q"} \tag{3}$$

where the average inlet ($T_{m,i}$) and outlet ($T_{m,o}$) temperature of the methanol is considered as the bulk fluid temperature inside the evaporator. R_{th} is the thermal resistance. The evaporator temperature ($T_{evaporator}$) is the average inlet, rear and outlet wall temperature of the evaporator. The thermal resistance plot for various heat fluxes is shown in Fig 21. From Fig 21, it can be observed

that the thermal resistance decreases with increasing heat flux up to 0.8 W/mm^2 and it slightly increases for the heat flux of 1 W/mm^2.

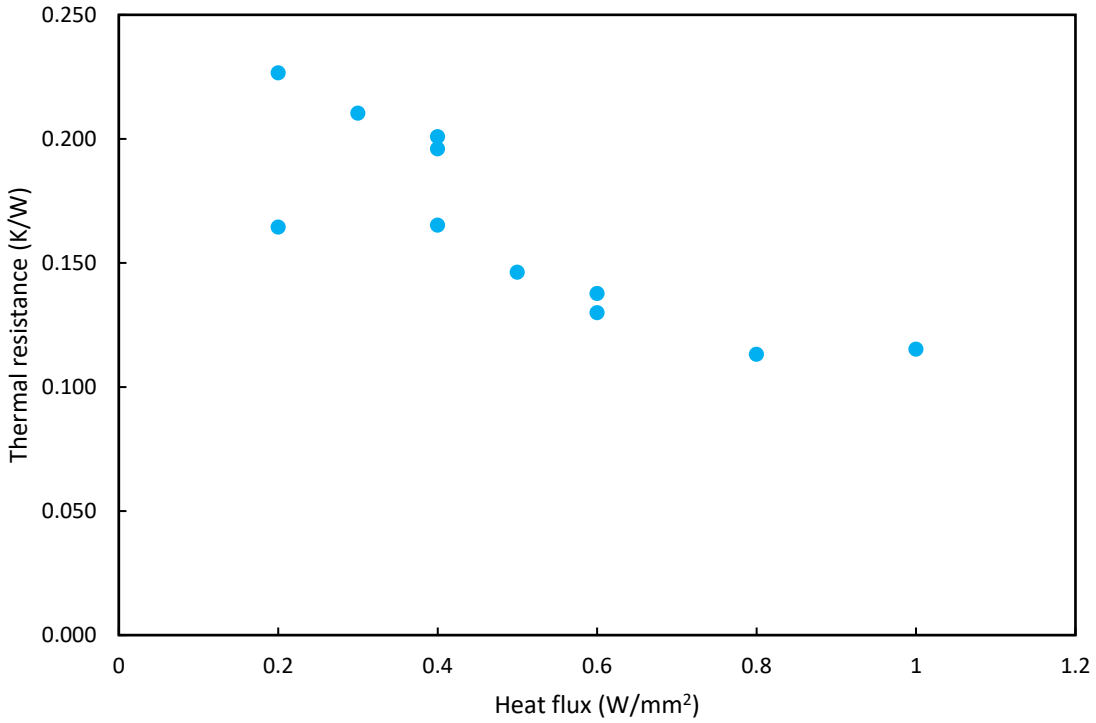

Fig. 21. Thermal resistance vs heat flux plot.

3.7. Ratio of applied heat to latent heat capacity

As noted previously, the important constraint for the operation of the system is that the minimum required mass flow rate of the system is obtained as the ratio of applied heat input to the latent heat capacity of the methanol. Since the evaporator is maintained at 5 kPa and 40 °C at the beginning of the flashing process, the inlet liquid temperature of ~20 °C denotes a superheated condition that can support the formation of both homogenous and heterogeneous nucleation. As the time taken for the methanol to contact the evaporator wall from the solenoid valve outlet is rapid, the influence of homogenous nucleation is assumed to be negligible. Case 2 depicts a scenario where the

supplied mass flow rate is less than the minimum required mass flow rate. This resulted in a continuous rise in temperature and steady periodic conditions were not achieved as the system temperature limit was reached.

The ratio of heat input to latent heat availability can be mathematically expressed in Eq. (4)

$$\eta = \frac{q}{\dot{m}\, h_{fg}} \tag{4}$$

The higher the η ratio, the more efficient the flash cooling or the higher the quality of vapor. This also acts as a measure of how much heat is extracted as the latent heat capacity of liquid. The plot of η with respect to heat flux is depicted in Fig 22. It can be observed that η is highest for heat fluxes from 0.2 to 0.5 W/mm^2 but for all the heat fluxes above 0.5 W/mm^2, the value of η ranges between 0.6 to 0.8. The η value can be increased for higher heat fluxes by operating at lesser t_{ON} time and for a shorter pulse cycle time such that the flow rate can be reduced without forming a stable vapor film.

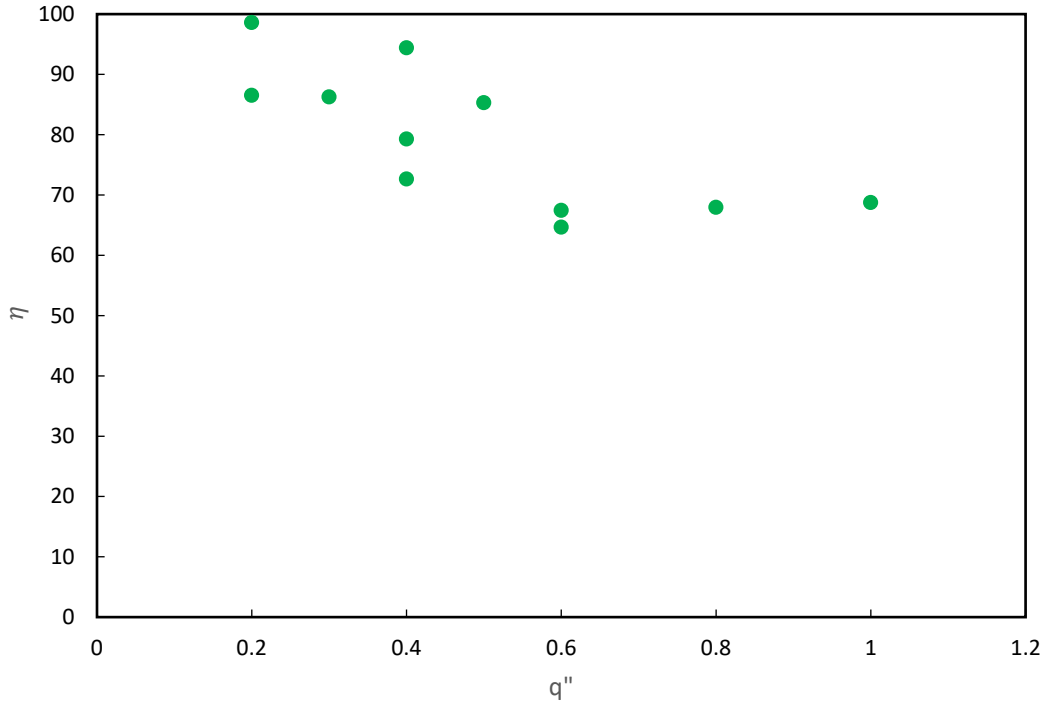

Fig. 22. The ratio of heat input to latent heat availability as a function of heat flux.

3.8. Role of evaporator design

The design of the evaporator is the key to determining the two-phase flow regime in addition to the heated zone. In the proposed evaporator, the heat is transferred from the heater to the evaporator in a vertically upward direction and the thermal gradient exists in the same direction. Therefore, the various flow boiling regimes in a cylindrical tube may not be applicable because the heat is applied radially in a typical flow boiling. In the proposed approach, the formation of vapor film is most likely to be at the bottom of the evaporator where the wall superheat is the highest. Meanwhile, the side and top walls will have lesser wall superheat but still sufficient to induce heterogeneous nucleation at higher heat fluxes.

3.9. Correlation of control parameters

The objective of this section is to determine the feasible values of control parameters given the heat flux to be cooled. Any engineering application would require such a model. In this section, the experimental data is correlated with the control parameters including heat flux, pulse cycle time and flow rate. From the experiments, it can be observed that a rise in the flow rate reduces the steady periodic temperature of the evaporator but after a particular flow rate, the rate of decrease in temperature tends to be asymptomatic. A similar correlation is observed between pulse cycle time and the steady periodic temperature of the evaporator. This is attributed to the high correlation between pulse cycle time and the flow rate. The experimental data of pulse cycle time and its corresponding flow rate is plotted in Fig 23. With curve fitting, the best profile is identified to be logarithmic with an R^2 value of 0.945. The experimental correlation between flow rate and pulse cycle time is estimated as Eq. (5). Eq. (5) maps the influence of pressure gradient-driven flow rate.

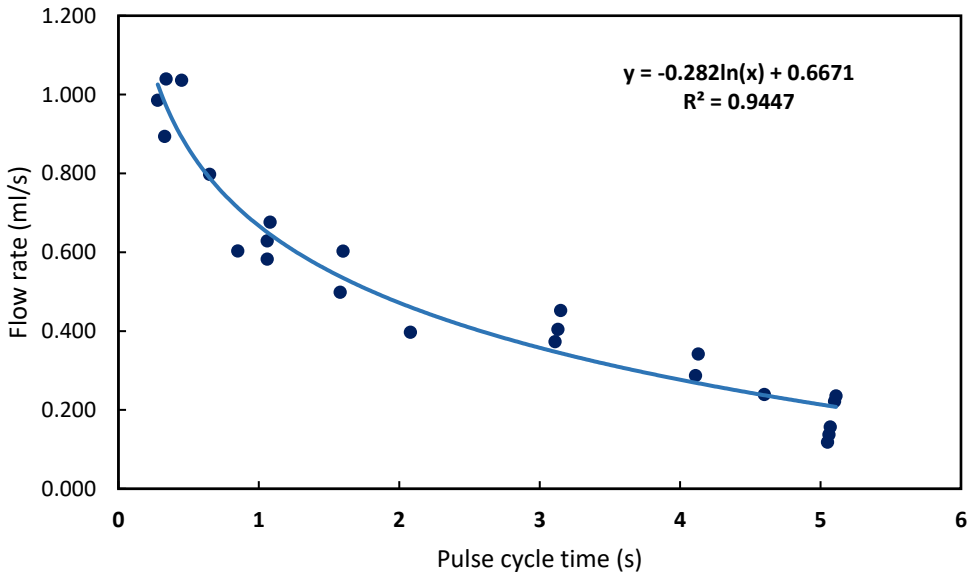

Fig. 23. Experimental correlation between flow rate and pulse cycle time.

$$\dot{\forall} = -0.282\ ln\ (t_p) + 0.6671 \tag{5}$$

where $\dot{\forall}$ is the flow rate and t_p is the pulse cycle time. As the cooling effect is a function of applied heat and the flow rate, a correlation between them would be helpful to relate all three control parameters. A plot between the heat flux and the flow rate is shown in Fig 24. The correlation between heat flux and flow rate yields Eq. (6). Using Eq. (6), we can determine the required flow rate for a given heat flux.

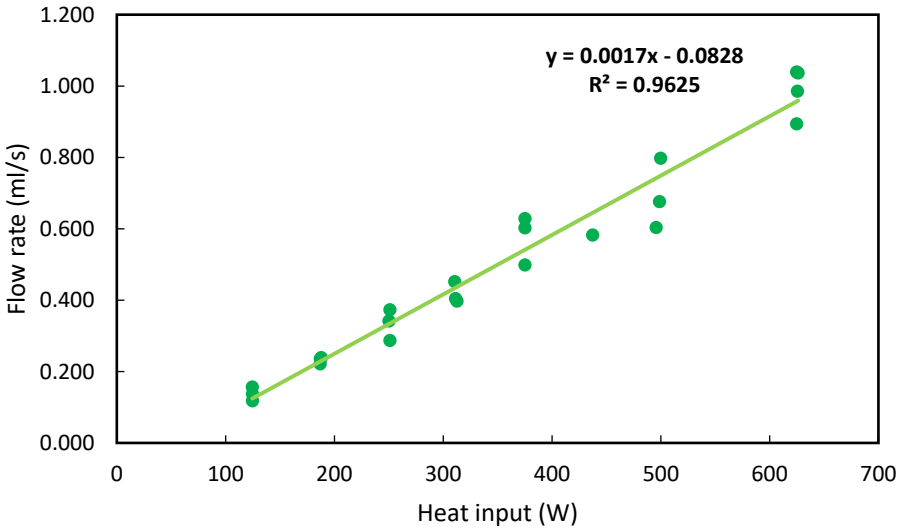

Fig. 24. Experimental correlation between flow rate and heat input.

$$\dot{\forall} = 0.0017(q) - 0.0828 \tag{6}$$

It should be noted that $\dot{\forall}$ should be greater than $\dot{\forall}_{min}$ which is represented in Eq. (6).

$$\dot{\forall} > \dot{\forall}_{min} = \frac{q}{\rho\, h_{fg}} \tag{7}$$

where q is the heat input in Watts, ρ is the density of the operating liquid and h_{fg} is the latent heat capacity of operating liquid in J/kg. Correlation between pulse cycle time and heat input can be obtained by equating Eq. (5) and (6). Upon simplification, we get Eq. (8).

$$\ln(t_p) = -0.006\,(q) + 2.659 \tag{8}$$

Eq. (8) will provide the maximum feasible pulse cycle time that does not support the stable vapor film formation to hinder the nucleation for a given heat input.

For translating the pulse cycle time into its components, t_{ON} and t_{OFF} timings, a correlation between t_{ON} and volume per pulse will be useful. A plot of volume per pulse versus t_{ON} is depicted in Fig 25. The experimental correlation provides a linear trend as given in Eq. (9).

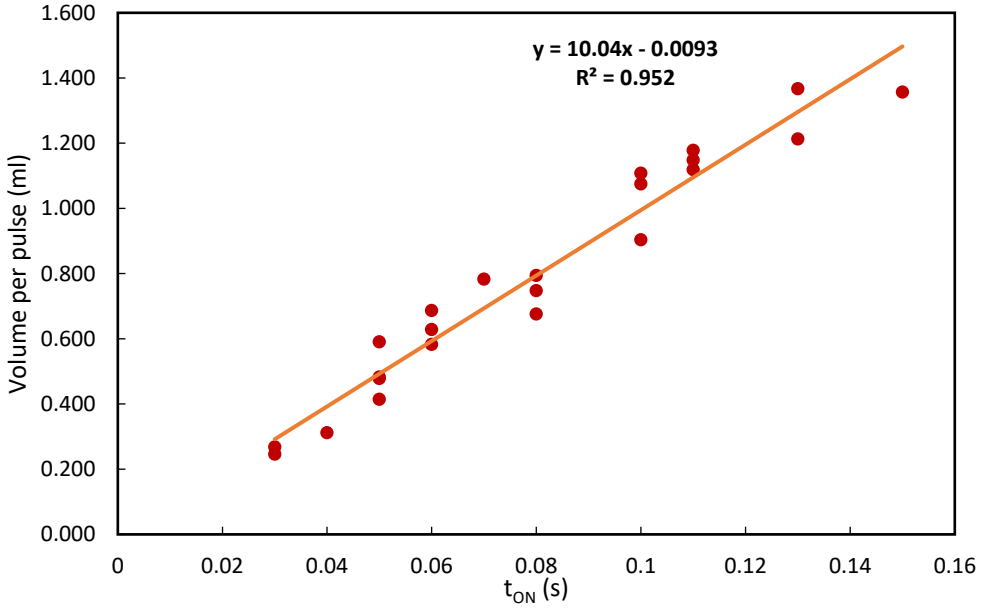

Fig. 25. Experimental correlation between volume per pulse and t_{ON}.

$$V_p = 10.04\,(T_{ON}) - 0.0093 \tag{9}$$

where V_p is the volume per pulse. If Eq. (9) is divided by t_p (pulse cycle time), then it will yield a time-averaged flow rate, $\dot{\forall}$. Therefore, once t_p is known for a given q using Eq. (8), the required flow rate can be determined by using Eq. (5). The obtained flow rate if multiplied by pulse cycle time, then it will yield volume per pulse. With volume per pulse, t_{ON} can be determined by using Eq. (9). t_{OFF} is the difference between t_p and t_{ON}. Using the discussed approach, the operating

conditions or the values of control parameters of pulsed flash cooling can be obtained. It is noteworthy that these operating conditions correspond to the maximum limit of pulse cycle time and corresponding minimum flow rate that is sufficient to achieve steady periodic conditions. To further improve the performance or reduce the steady periodic temperature, a lower pulse cycle time and higher flow rate values can be utilized.

With the experiments, it was observed that pulse cycle time is the dominant control parameter and only if it is below a certain limit, the pulsed flash cooling achieves steady periodic conditions irrespective of the flow rates for a given heat flux. The pulse cycle time limit is determined and reported in Table 10 by following the discussed method using Eqs. (5), (8) and (9).

Table 10. Determination of minimum feasible operating conditions for each heat flux

Heat flux	**Heat input**	$\mathbf{t_{p,\,max}}$	**Flow rate**	$\mathbf{V_p}$	$\mathbf{t_{ON}}$	$\mathbf{t_{OFF}}$
W/mm^2	**W**	**s**	**ml/s**	**ml**	**s**	**s**
0.2	125	6.75	0.1288	0.869	0.09	6.66
0.3	187.5	4.64	0.2345	1.087	0.11	4.53
0.4	250	3.19	0.3403	1.084	0.11	3.08
0.5	312.5	2.19	0.4460	0.977	0.10	2.09
0.6	375	1.51	0.5518	0.831	0.08	1.42
0.7	437.5	1.03	0.6575	0.680	0.07	0.97
0.8	500	0.71	0.7633	0.543	0.05	0.66
0.9	562.5	0.49	0.8690	0.425	0.04	0.45
1	625	0.34	0.9748	0.327	0.03	0.30

It is put forward that if the pulse cycle time is maintained below the determined t_p in Table 10, then better performance in terms of lower thermal resistance can be achieved. If the pulse cycle time is maintained above the t_p values in Table 10, then the possibility of stable vapor film formation is higher, especially for higher heat fluxes.

Chapter 4. Summary and conclusions

Thermal management of high heat flux electronics, especially wafer-scale systems present intricate challenges by dissipating greater than 0.5 W/mm^2 heat flux and cooling should be achieved without heat spreading. The required heat transfer coefficients are achievable only by two-phase cooling techniques and this study considers flash cooling approach as a solution. Flash cooling is a boiling phenomenon driven by pressure control. A considerable amount of research is focused on vacuum spray flash cooling and pool flash boiling but none of the work is tailored for high heat flux electronic cooling with methanol at low flow rates. Furthermore, this work aims to understand the flash cooling phenomenon both from a physics and engineering perspective.

A closed-loop flash cooling system is developed, and the components of the closed-loop include evaporator, accumulator, vacuum pump, condenser, methanol reservoir and peristaltic pump. Eight thermocouples and three pressure transducers are employed, and the data is acquired and stored using LabVIEW software. The pulsed flow flash boiling is achieved by installing a solenoid valve between the evaporator and the reservoir while the solenoid valve is controlled by a relay module following the coding command in LabVIEW. The heat flux varied from 0.2 W/mm^2 to 1 W/mm^2 and for each heat flux, experiments were conducted until at least one experimental case achieved steady-periodic conditions. The influence of flow rate and pulse cycle time is also observed by varying these parameters.

Among the three control parameters (heat flux, pulse cycle time and flow rate), it was observed that pulse cycle time is the dominant parameter that provides a limit to achieve steady-periodic conditions. A higher pulse cycle time for high heat fluxes creates a favorable situation for stable

vapor film formation and baffles the heat transfer. This observation is evident even if the flow rate is increased by raising the t_{ON} time of the solenoid valve without changing the t_{OFF} time. Nevertheless, the evaporator can be recovered from partial dry-out conditions just by increasing the pulse frequency or decreasing the pulse cycle time to achieve steady-periodic conditions. The control offered by the system is commendable for transient and dynamic cooling of wafer-scale systems. Furthermore, the control parameters are correlated with each other and the feasible pulse cycle time for a given heat flux is determined. From an engineering perspective, the system can be upgraded to include a PID algorithm to decide a pulse cycle time using the developed correlation for given heat flux and required operating temperature.

The future direction of flash cooling technology can be focused on understanding the flashing phenomena during dry-out conditions or operating near critical heat flux conditions. The design of experiments can be extended to analyze the influence of lower pulse cycle time and its relationship with its thermal resistance. Such experiments can aid in providing an accurate numerical model to run the system to achieve a defined steady periodic temperature. Furthermore, the oscillation range can be mapped to flow rate and pulse cycle time for a given heat flux to identify a relationship between them. Another set of experiments can be designed to compare continuous and pulsed flow flash cooling. In conclusion, a stable closed-loop flash cycle is developed, and the characteristics of flash cooling are reported with respect to heat flux, pulse time and flow rate.

References

1. Z. Zhang, X. Wang, and Y. Yan. “A review of the state-of-the-art in electronic cooling”, e-Prime - Advances in Electrical Engineering, Electronics and Energy 1 (2021): 100009.
2. M. Iyengar, Energy Consumption of Information Technology Data Centers, Electronics Cooling, Accessed on: 18 November 2023 [Online]. Available: https://www.electronics-cooling.com/2010/12/energy-consumption-of-information-technology-data-centers/#:~:text=The%20IT%20equipment%20usually%20consumes,of%20the%20total%20energy%20use.
3. S. S. Murshed, and C. N. De Castro. “A critical review of traditional and emerging techniques and fluids for electronics cooling” Renewable and Sustainable Energy Reviews, 78 (2017): 821-833.
4. NVIDIA, H100, Access on: 18 November 2023 [Online]. Available: https://www.nvidia.com/en-us/data-center/h100/
5. S. S. Iyer, "Heterogeneous Integration for Performance and Scaling" IEEE Transactions on Components, Packaging and Manufacturing Technology, vol. 6, no. 7, (2016): pp. 973-982,
6. A. A. Bajwa, S. Jangam, S. Pal, N. Marathe, T. Bai, T. Fukushima, M. Goorsky and S. S. Iyer, "Heterogeneous Integration at Fine Pitch ≤ 10 μm Using Thermal Compression Bonding," in IEEE 67th Electronic Components and Technology Conference (ECTC), Orlando, FL, USA, 2017.
7. H. Ren, K. Sahoo, T. Xiang, G. Ouyang and S. S. Iyer, "Demonstration of a Power-efficient and Cost-effective Power Delivery Architecture for Heterogeneously Integrated Wafer-scale Systems," *2023 IEEE 73rd Electronic Components and Technology Conference (ECTC)*, Orlando, FL, USA, 2023, pp. 1614-1621.

8. L. Pietrasanta. “Experimental analysis of two-phase flows in the context of Pulsating Heat Pipes for space applications” Thesis, University of Brighton (2019). 10.13140/RG.2.2.26001.66401
9. U. Shah, “Transient analysis of flash cooling for dynamic thermal management for high-performance electronic systems,” 2023, *UCLA*. ProQuest ID: Shah_ucla_0031D_22162. Merritt ID: ark:/13030/m5vv0wz2. Retrieved from https://escholarship.org/uc/item/8510z7zd
10. G. Venkatesan, S. Iniyan, and R. Goic, “A prototype flash cooling desalination system using cooling water effluents.” International Journal of Energy Research, 37 (2013): 1132-1140.
11. H. Fu, R. Zhao, W. Long, and W. Cheng. "Study on cooling performance of rapid cooling system based on vacuum spray flash evaporation." *Applied Thermal Engineering* 201 (2022): 117751.
12. W.-L. Cheng, Y.-H. Peng, H. Chen, L. Hu, and H.-P. Hu. "Experimental investigation on the heat transfer characteristics of vacuum spray flash evaporation cooling." *International Journal of Heat and Mass Transfer* 102 (2016): 233-240.
13. Y.-H. Peng, and W.-L. Cheng. "Experimental investigation on the effect of heat transfer enhancement of vacuum spray flash evaporation cooling using Al2O3–water nanofluid." *Energy Procedia* 142 (2017): 3766-3773.
14. Z.-F. Zhou, Y.-K. Lin, H.-L. Tang, Y. Fang, B. Chen, and Y. -C. Wang. "Heat transfer enhancement due to surface modification in the close-loop R410A flash evaporation spray cooling." *International Journal of Heat and Mass Transfer* 139 (2019): 1047-1055.
15. D. Kawano, H. Ishii, H. Suzuki, Y. Goto, M. Odaka and J. Senda, "Numerical Study on Flash-Boiling Spray of Multicomponent Fuel," Heat Transfer-Asian Research, 35 (2006): 369-385.

16. W.-L. Cheng, W.-W. Zhang, H. Chen, and L. Hu. "Spray cooling and flash evaporation cooling: The current development and application." *Renewable and Sustainable Energy Reviews* 55 (2016): 614-628.
17. W.-l. Cheng, H. Chen, L. Hu, and W.-w. Zhang. "Effect of droplet flash evaporation on vacuum flash evaporation cooling: Modeling." *International Journal of Heat and Mass Transfer* 84 (2015): 149-157.
18. G. Guo, and C. Zhu. "A modified lumped heat capacity model for droplet flash cooling." *International Communications in Heat and Mass Transfer* 127 (2021): 105557.
19. Q. Zhang, Q. Bi, J. Wu, J. Liang and W. Wang, “Experimental investigation on the rapid evaporation of high-pressure R113 liquid due to sudden depressurization," International Journal of Heat and Mass Transfer, 61 (2013): 646-653.
20. I. Aoki. "Analysis of characteristics of water flash evaporation under low-pressure conditions." *Heat Transfer—Asian Research: Co-sponsored by the Society of Chemical Engineers of Japan and the Heat Transfer Division of ASME* 29, no. 1 (2000): 22-33.
21. J.D. Engerer, J.H. Doty, and T.S. Fisher. "Transient thermal analysis of flash-boiling cooling in the presence of high-heat-flux loads." *International Journal of Heat and Mass Transfer* 123 (2018): 678-692.
22. J. Mathew and S. Krishnan, "A Review on Transient Thermal Management of Electronic Devices," ASME. J. Electron. Packag. , 144 (2022): 010801.
23. Schlenker, E. L. , 2018, “ Modeling and Characterization of High-Power Electronic Devices: System Analysis of Laser Diodes With Flash Boiling and GAN HEMT Reliability Modeling,” M.S. thesis, Purdue University, West Lafayette, IN.https://docs.lib.purdue.edu/dissertations/AAI10823098/"

24. U. Shah, S.S. Iyer, and T.S. Fisher. "Segmented Thermal Management with Flash Cooling for Heterogeneous Wafer-Scale Systems." In *2021 20th IEEE Intersociety Conference on Thermal and Thermomechanical Phenomena in Electronic Systems (iTherm)*, (2021) 589-594.
25. U. Shah, U. Mogera, P. Ambhore, B. Vaisband, S. S. Iyer and T. S. Fisher, "Dynamic Thermal Management Of Silicon Interconnect Fabric Using Flash Cooling," in 18th IEEE Intersociety Conference on Thermal and Thermomechanical Phenomena in Electronic Systems (ITherm), Las vegas, NV, USA, 2019.
26. M. X. Ma, "Experimental Investigation of Pressure-Controlled Boiling for Rapid Transient Cooling," University of California, Los angeles, 2021.
27. U. Shah, M. Ma, M. T. B.-C. ,. Barako, S. S. Iyer and T. S. Fisher, "Experimental Demonstration of Pressure-Driven Flash Boiling for Transient Two-Phase Cooling," IEEE Transactions on Components, Packaging and Manufacturing Technology, 11 (2021): 1604-1614.
28. J. D. Engerer and T. S. Fisher, "Flash boiling from carbon foams for high-heat-flux transient cooling," Applied Physics Letters, 109 (2016): 024102
29. J. D. Engerer, "Rapid transient cooling utilizing flash boiling and desorption on graphitic foams," Purdue University, West lafayette, IN, USA, 2016.
30. S. Singh, P.R. Chakraborty, and H.B. Kothadia. "Flash evaporation method for improved desalination and cooling applications: An experimental study." *Desalination* 566 (2023): 116933.

31. S. Singh, P.R. Chakraborty, and H.B. Kothadia. "Experimental study on energy transformation of static liquid pool during flash evaporation." *Applied Thermal Engineering* 220 (2023): 119712.
32. Custom thermoelectric, Water block, Access on: 18 November 2023 [Online]. Available: https://customthermoelectric.com/water-block-1-0-x-1-0-x-0-49-copper.html
33. Watlow, Ceramic Heater, Access on: 18 November 2023 [Online]. Available: https://www.thermaldevices.com/product/watlow-ultramic-240-volt-967-watt-ceramic-heater-cer-1-01-00002/
34. Omega, OmegaTherm201, Access on: 18 November 2023 [Online]. Available: https://assets.omega.com/pdf/consumables/adhesives-and-paste/OT-201.pdf
35. Pyrogel, Aerogel Insulator, Access on: 18 November 2023 [Online]. Available: http://www.buyaerogel.com/wp-content/uploads/2017/09/Pyrogel-XTE-Datasheet.pdf
36. McMaster, Calcium Silicate insulator, Access on: 18 November 2023 [Online]. Available: https://www.mcmaster.com/products/insulation/
37. Marshall Scientific, Edward Vacuum pump, Access on: 18 November 2023 [Online]. Available: https://www.marshallscientific.com/Edwards-RV3-Rotary-Vane-Vacuum-Pump-p/ed-rv3.htm
38. Packless, Condenser coil, Access on: 18 November 2023 [Online]. Available: https://packless.com/products/condenser-wshp-coils/coax-2201-j
39. Granzow, Solenoid valve, Access on: 18 November 2023 [Online]. Available: https://www.granzow.com/valves/solenoid/A2D41-00T-05B
40. Magna-Power, DC Power supply equipment, Access on: 18 November 2023 [Online]. Available: https://magna-power.com/products/magnadc/ts